Semiclassical transport in nearly symmetric quantum dots I: symmetry-breaking in the dot

Robert S. Whitney,[1] Henning Schomerus,[2] and Marten Kopp[2]

[1]*Institut Laue-Langevin, 6 rue Jules Horowitz, B.P. 156, 38042 Grenoble, France*
[2]*Department of Physics, Lancaster University, Lancaster, LA1 4YB, United Kingdom*

(Dated: June 4, 2009)

We apply the semiclassical theory of transport to quantum dots with exact and approximate spatial symmetries; left-right mirror symmetry, up-down mirror symmetry, inversion symmetry or four-fold symmetry. In this work — the first of a pair of articles — we consider (a) perfectly symmetric dots and (b) nearly symmetric dots in which the symmetry is broken by the dot's internal dynamics. The second article addresses symmetry-breaking by displacement of the leads. Using semiclassics, we identify the origin of the symmetry-induced interference effects that contribute to weak localization corrections and universal conductance fluctuations. For perfect spatial symmetry, we recover results previously found using the random-matrix theory conjecture. We then go on to show how the results are affected by asymmetries in the dot, magnetic fields and decoherence. In particular, the symmetry-asymmetry crossover is found to be described by a universal dependence on an asymmetry parameter $\gamma_{\rm asym}$. However, the form of this parameter is very different depending on how the dot is deformed away from spatial symmetry. Symmetry-induced interference effects are completely destroyed when the dot's boundary is globally deformed by less than an electron wavelength. In contrast, these effects are only reduced by a finite amount when a part of the dot's boundary smaller than a lead-width is deformed an arbitrarily large distance.

PACS numbers: 05.45.Mt,74.40.+k,73.23.-b,03.65.Yz

I. INTRODUCTION

In recent years there has been a great deal of progress in using semiclassical methods to describe the quantum behaviour of systems which are classically chaotic. Semiclassics was applied to analyzing the transport properties of chaotic quantum dots in Refs. [1, 2]. Despite clear indications from the quasiclassical method [3, 4, 5, 6], it took many years to understand how to go beyond the diagonal approximation [7, 8, 9], and thereby use semiclassics to analyze mesoscopic effects such as weak localization [10, 11, 12, 13], universal conductance fluctuations [14, 15] and shot-noise [16, 17, 18]. Before these works, general statements on the quantum behaviour of such systems relied on the Bohigas-Giannoni-Schmit conjecture [19] that they are well-described by random-matrix theory (RMT) [20, 21]. RMT is a statistical theory based on the assumption that we know nothing about the dynamics of the system (besides global symmetries such as time-reversal and spin-rotation symmetry). However, often this is not the case; perhaps the system has extra constants of motion or the classical phase space of the system is mixed (so that some parts are regular and others are chaotic). Such systems are hard to treat using RMT methods. In those cases where progress with RMT is possible, one adds more phenomenological parameters to the theory, thereby reducing its predictive power. One of the great hopes for semiclassics is that it will provide *microscopic* theories for such situations, in which all parameters can be derived from properties of the confining potential (and any inter-particle interactions that are present).

A simpler, but related, problem is that of chaotic systems with additional spatial symmetries (reflection or inversion symmetries). One can ask two questions. Do spatial symmetries lead to interference effects similar to those induced by time-reversal symmetry (coherent backscattering and weak localization effects)? If so, how are these interference effects changed by the presence of spatial asymmetries or magnetic fields?

These discrete spatial symmetries are simple enough to be amenable to a phenomenological analysis with RMT. Such an analysis was carried out in Refs. [22, 23] where it was shown that spatial symmetries do indeed lead to extra interference effects analogous to weak localization. Since that work, there have been a number of other studies of chaotic systems with symmetries. Refs. [24, 25, 26] use RMT methods to study the distribution of transmission eigenvalues, while Ref. [27] identifies a huge interference effect in double-dots separated by a tunnel barrier. However, none of these works have addressed how the weak localization correction and conductance fluctuations behave for dots that are only approximately symmetric.

This is the first of a pair of articles in which we perform a semiclassical analysis of symmetry-induced interference effects on quantum transport, and in particular their contributions to weak localization corrections and conductance fluctuations. We consider a quantum dot (billiard) whose shape has spatial symmetries (mirror or inversion symmetries) but is otherwise shaped such that the classical dynamics within it would exhibit hyperbolic chaos (exponential divergence of initially close trajectories). We develop a semiclassical theory of transport between two ideal leads coupled to the dot, building on the theory for similar chaotic systems without spatial sym-

	Average conductance		UCFs	
	$B \ll B_c$	$B \gg B_c$	$B \ll B_c$	$B \gg B_c$
no spatial sym.	$\frac{N}{2} - \frac{1}{4}$	$\frac{N}{2}$	$\frac{1}{8}$	$\frac{1}{16}$
left-right sym.	$\frac{N}{2}$	$\frac{N}{2} + \frac{1}{4}$	$\frac{1}{4}$	$\frac{1}{8}$
inversion sym.	$\frac{N}{2}$	$\frac{N}{2}$	$\frac{1}{4}$	$\frac{1}{8}$
up-down sym.	$\frac{N}{2} - \frac{1}{2}$	$\frac{N}{2} - \frac{1}{4}$	$\frac{1}{4}$	$\frac{1}{8}$
four-fold sym.	$\frac{N}{2}$	$\frac{N}{2}$	$\frac{1}{2}$	$\frac{1}{4}$

Table I: Table of the values of average conductance and conductance fluctuations for quantum dots with different spatial symmetries, attached to two leads both carrying $N \gg 1$ modes. B_c is a magnetic field strength at which time-reversal symmetry is broken in the asymmetric situation. These results are taken from Refs. [22, 23], where they were derived in RMT. Here we rederive these results semiclassically, and show how they depend on asymmetries in the dot, dephasing, magnetic fields and Ehrenfest times.

metries. First, we give a non-phenomenological explanation of the origin of the symmetry-induced interference effects found in RMT [22, 23]. We then investigate how transport is affected by asymmetries in the dot, magnetic fields, dephasing, and the Ehrenfest time (which characterizes the emergence of fully developed wave chaos [5, 28]). For this we make use of analogies with the analysis of dephasing in asymmetric dots [29, 30, 31].

We find that different types of deformations away from symmetry destroy the symmetry-induced interference effects in remarkably different ways. The deformations we consider have the same universal dependence on an asymmetry parameter $\gamma_{\rm asym}$; however, the microscopic form of this parameter varies depending on the type of deformation. For a global deformation of the dot (say half the dot is displaced outward), we find that a displacement δL of less than a Fermi wavelength is sufficient to completely destroy the symmetry-induced interference effects. In contrast, for the deformation of a small part of the boundary (say a portion less than but of order a lead-width is displaced outwards) we find that an arbitrary large displacement δL does not destroy the symmetry-induced interference effects completely, instead it simply suppresses them by a finite amount.

Finally, we address how asymmetries and magnetic fields can be incorporated into a simple phenomenological RMT model, and compare results of numerical computations in this model with the semiclassical predictions.

In the second of this pair of articles [32], we use the same methods to find these transport properties for a spatially symmetric system coupled to leads which do not respect the symmetry.

II. SCOPE AND OVERVIEW OF THIS WORK

In this article we consider two-dimensional chaotic quantum dots of characteristic size L, perfectly coupled to two leads, labeled the left (L) and right (R) lead. The leads have widths $W_{\rm L}$ and $W_{\rm R}$ much greater than the Fermi wavelength $\lambda_{\rm F} = h/p_{\rm F}$. Thus the leads carry $N_{\rm L}$ and $N_{\rm R}$ modes, where $N_\kappa = p_{\rm F} W_\kappa/(\pi\hbar) \gg 1$ for $\kappa \in {\rm L}, {\rm R}$.

Assuming that ergodicity of the classical dynamics is established quickly, there are only a few time scales which fully characterize the quantum transport through the dot. The typical time that a particle spends in the dot is given by the dwell time $\tau_{\rm D} = \tau_0 \times C/(W_{\rm L} + W_{\rm R})$, where C is the dot's circumference and $\tau_0 = \pi A/C v_F$ is the scattering time off the boundary (here A is the area of the dot and v_F is the Fermi velocity).

It is now clear that the development of quantum interference effects in such systems is governed by Ehrenfest times $\tau_{\rm E}$ [5]. Semiclassics enables us to treat finite Ehrenfest times, thereby exploring the crossover between RMT behaviour ($\tau_{\rm E} \ll \tau_{\rm D}$) and classical behaviour ($\tau_{\rm E} \gg \tau_{\rm D}$). There is in fact a set of Ehrenfest times, which all take the form [28]

$$\tau_{\rm E} = \Lambda^{-1} \ln[(L/\lambda_{\rm F})\mathcal{L}] \qquad (1)$$

where Λ is the Lyapunov exponent of the classical dynamics in the dot, and $\mathcal{L}$ is the ratio of characteristic classical length scales. Of relevance for this paper are the open-system Ehrenfest time $\tau_{\rm E}^{\rm o}$, given by Eq. (1) with $\mathcal{L} = (W/L)^2$ [33], and the closed-system Ehrenfest time $\tau_{\rm E}^{\rm c}$ with $\mathcal{L} = 1$ (a third Ehrenfest time $\tau_{\rm E}^{\rm d}$ with $\mathcal{L} = W/L$ is relevant for decay problems [34]).

Two other relevant time scales are the dephasing time $\tau_\phi = 1/\gamma_\phi$ (where γ_ϕ is the dephasing rate), and the time scale $\tau_B \sim (B_0/B)^2 \tau_0$ on which a magnetic field destroys time-reversal symmetry in the internal dynamics. Here, $B_0 \sim h/(eA)$ is a characteristic field strength at which about one flux quantum penetrates the quantum dot. For transport, the effect of a magnetic field is significant when it is of order

$$B_c = a B_0 \sqrt{\tau_0/2\tau_{\rm D}}, \qquad (2)$$

where a is a system-specific parameter of order one [21].

There are three spatial symmetries of particular interest for transport through a chaotic quantum dot coupled to two leads. The first two map the L lead onto the R lead and vice versa, they are a left-right mirror symmetry (Fig. 2) and an inversion symmetry (Fig. 4). The third type of symmetry maps each lead onto itself, such as an up-down mirror symmetry (Fig. 5). A dot with any two of the three symmetries listed above is four-fold symmetric, and automatically satisfies the third symmetry. Four-fold symmetry is most easily visualized by considering a dot which has both left-right and up-down mirror symmetry. For dots with two leads there are no additional cases of multiple symmetry.

Readers already familiar with the semiclassical theory of weak localization [10] and coherent backscattering [12, 13] may only need to look at Figs. 2-5 to understand the extra symmetry-induced interference effects. Once one folds the paths shown under the relevant symmetry (the right-hand sketches in each figure), we obtain contributions which are similar to the weak localization and coherent backscattering contributions in a system with no spatial symmetries. Indeed, given these figures, many such readers will probably be able to correctly guess the form of the results for perfect symmetry, which agree with the results of RMT tabulated in Table I. Treating asymmetries, however, is more involved.

The rest of this article is laid out as follows. In Section III we review the semiclassical description of quantum transport, and discuss how it should be modified to include spatial symmetries. In Section IV we treat weak localization in dots with left-right symmetry and discuss the role of perpendicular magnetic fields, dephasing, and asymmetry in the dot. In Sections V, VI and VII we analyze weak localization in dots with inversion symmetry, up-down symmetry and four-fold symmetry, respectively.

In Section VIII we provide a semiclassical description of conductance fluctuations in symmetric systems and discuss the effects of asymmetries and perpendicular magnetic fields. To keep the discussion simple we do not address dephasing here (unlike for weak localization).

In Section IX we propose an efficient phenomenological model to study symmetry breaking in RMT and compare the results of numerical computations to the semiclassical predictions.

Finally in Section X, we consider the application of our results to experimental systems. We estimate the necessary conditions for observing these symmetry-induced effects in the transport of electrons through quantum dots, and of microwaves through chaotic cavities.

III. THE THEORY OF SEMICLASSICAL TRANSPORT

The semiclassical picture of weak localization in disordered systems has been known for many years for both s-wave disorder [3, 4] and smooth disorder [5]. However, only recently has it been possible to extend this picture to disorder-free but chaotic systems, such as ballistic quantum dots [10]. We start with the semiclassical theory of transport [1, 2] and sum over lead modes as in Ref. [12] (see also Appendix B in Ref. [35]). Then the dimensionless conductance (conductance in units of $2e^2/h$) is given by

$$g \;=\; \frac{1}{2\pi\hbar}\int_{\rm L}\mathrm{d}y_0\int_{\rm R}\mathrm{d}y\sum_{\gamma,\gamma'}A_\gamma A_{\gamma'}\;\; e^{i(S_\gamma-S_{\gamma'})/\hbar}, \quad (3)$$

where the double sum is over all classical paths γ,γ', from point y_0 on lead L to point y on lead R. Path γ has a classical action $S_\gamma = \int_\gamma \mathbf{p}\mathrm{d}\mathbf{r}$, and an amplitude A_γ. Refs. [1, 2] have shown that the squared-amplitude $A_\gamma^2 = (\mathrm{d}p_{y0}/\mathrm{d}y)$, so it measures the path's stability (the change in the path's initial momentum p_{y0} associated with a small displacement of its final position y).

For most pairs of γ and γ' the exponential in Eq. (3) oscillates wildly as one changes the energy or the dot-shape. Thus they make no contribution to the average conductance (where one averages over energy, dot-shape, or both). The only contributions that survive averaging are those where the pairs of paths have highly correlated actions; typically one has $S_\gamma \simeq S_{\gamma'}$ for a broad range of energies and dot-shapes. The simplest example of this are all contributions to the double-sum with $\gamma' = \gamma$. These "diagonal contributions" to the above double sum can be evaluated with the help of the sum rule (in the spirit of Eq. (B6) of Ref. [1])

$$\sum_\gamma A_\gamma^2\,[\cdots]_\gamma \;=\; \int_{-\frac{\pi}{2}}^{\frac{\pi}{2}}\mathrm{d}\theta_0\int_{-\frac{\pi}{2}}^{\frac{\pi}{2}}\mathrm{d}\theta\, p_{\rm F}\cos\theta_0 \times\tilde{P}(\mathbf{Y},\mathbf{Y}_0;t)\,[\cdots]_{\mathbf{Y}_0}\,, \quad (4)$$

where we define $\tilde{P}(\mathbf{Y},\mathbf{Y}_0;t)\delta y\delta\theta\delta t$ as the classical probability for a particle to go from an initial position and momentum angle of $\mathbf{Y}_0 \equiv (y_0,\theta_0)$ on lead L to within $(\delta y,\delta\theta)$ of $\mathbf{Y} = (y,\theta)$ on lead R in a time within δt of t. For any given dot at a given energy, $\tilde{P}(\mathbf{Y},\mathbf{Y}_0;t)$ has a Dirac δ-function on each classical path. However, the average of $\tilde{P}$ over an ensemble of dots or over energy gives a smooth function. We assume the classical dynamics exhibit hyperbolic chaos, thus they will be mixing. If the dynamics are mixing on a timescale $\ll \tau_{\rm D}$, this function will rapidly decay to a uniform distribution over phase space, so that we can assume $\left\langle\tilde{P}(\mathbf{Y};\mathbf{Y}_0;t)\right\rangle = e^{-t/\tau_{\rm D}}\cos\theta/(2\,(W_{\rm L}+W_{\rm R})\,\tau_{\rm D})$. The sum of these diagonal contributions gives the Drude conductance (also called the classical conductance)

$$\langle g\rangle_{\rm D} = \frac{N_{\rm L}N_{\rm R}}{(N_{\rm L}+N_{\rm R})}. \quad (5)$$

A. Weak localization

Systems that exhibit time-reversal symmetry (typically systems in zero magnetic field) have correlations between paths that are the time-reverse of each other. If path γ' is the time-reverse of path γ then $S_\gamma = S_{\gamma'}$ for all energies and dot-shapes, and as such one could expect contributions to the average conductance coming from these pairs of paths. However, looking at Eq. 3, we see that paths that are the *exact* time-reverse of each other contribute to reflection but not transmission, and further require that $y = y_0$ which reduces their contribution to reflection to zero. In contrast, paths that are the *approximate* time-reverse of each other, or have segments that are the approximate time-reverse of each other, give a finite contribution to both reflection and transmission.

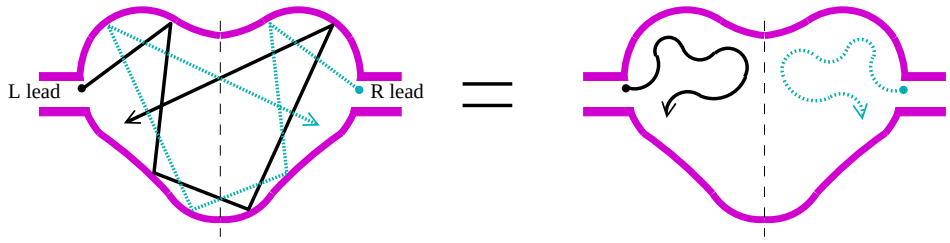

Figure 1: (colour online). Sketch of a planar quantum dot with a left-right mirror symmetry. On the left we show a classical path (solid line) and its mirror image (dashed line). Each path is piecewise straight and undergoes specular reflections at the boundary of the dot. The path is chaotic (we assume hyperbolic chaos), so its position and momentum after time t are exponentially sensitive to the initial position and momentum. We assume the system is such that a typical path crosses the symmetry axis a large number of times before escaping into a lead (these crossings occur on a timescale of order of the time-of-flight across the system). To simplify the sketches elsewhere in this article we draw paths as abstract curves (shown on the right) which only show those crossings of the symmetry axis which are crucial to the nature of the path.

They are the weak localization and coherent backscattering contributions discussed in Ref. [10], with the latter being more carefully analyzed in Refs. [12, 13]. Such contributions all involve a path γ having a loop such that there is an *encounter* where the path comes very close to itself while *also* having the opposite momentum (resulting in two almost-parallel segments which are traversed in opposite direction). Path γ' closely follows γ, but traverses the loop in opposite direction, which results in a crossing at the encounter. For classical dynamics which exhibit hyperbolic chaos, $|S_\gamma - S_{\gamma'}| < \hbar$ for all energies and dot-shapes if at the encounter the two parallel segments of path γ are separated by a distance less than $(\lambda_F L)^{1/2}$. Thus such contributions survive averaging, and summing them gives the weak localization correction to the average conductance,

$$\langle \delta g \rangle_{\rm wl} = -\frac{N_L N_R}{(N_L+N_R)^2} \exp[-\tau_E^c/\tau_D] \times Z(B,\gamma_\phi). \quad (6)$$

The RMT regime is defined by $\tau_E^c \ll \tau_D$ so that the factor $\exp[-\tau_E^c/\tau_D]$ equates to unity. In the classical regime ($\tau_E^c > \tau_D$), on the other hand, the weak localization correction is exponentially suppressed [5]. The factor

$$Z(B,\gamma_\phi) \;=\; \frac{\exp[-\gamma_\phi \tilde{\tau}]}{1+(B/B_c)^2+\gamma_\phi \tau_D} \quad (7)$$

describes the suppression due to a magnetic field and finite dephasing. The magnetic-field induced suppression occurs with the crossover from dynamics with time-reversal symmetry to dynamics without time-reversal symmetry. The crossover scale B_c is given in Eq. (2).

The time scale $\tilde{\tau}$ depends on the origin of the dephasing [29, 30, 31]. For electron-electron interactions $\tilde{\tau}$ in the dot [29] or dephasing leads [30] it is of order the Ehrenfest time, while for dephasing due to microwave noise or charge-fluctuations on gates near the dot it is given by the logarithm of the ratio of the noise correlation length, ξ, to the dot size. See Ref. [31] for an extensive discussion of the nature of ξ and $\tilde{\tau}$ for all these sources of noise.

B. Universal conductance fluctuations (UCFs)

The conductance of an individual quantum dot has a characteristic dependence on energy, applied magnetic field, and deformations of the dot's shape (which can be controlled by the voltages applied to the side- or top gates providing the electrostatic confinement). The magnitude of these fluctuations can be characterized by the variance of the conductance, which "universally" has a magnitude of order $(e^2/h)^2$ (meaning the variance of the dimensionless conductance is of order 1). In the absence of dephasing, semiclassics predicts UCFs in a chaotic quantum dot with no spatial symmetries given by [14, 15]

$${\rm var}(g) = \frac{N_L^2 N_R^2}{(N_L+N_R)^4} \times Z_{\rm ucf}(B), \quad (8)$$

where

$$Z_{\rm ucf}(B) = 1 + \frac{{\rm e}^{-\tau_E^o/\tau_D}}{[1+(B/B_c)^2]^2} + \frac{1-{\rm e}^{-\tau_E^o/\tau_D}}{1+(B/B_c)^2} \quad (9)$$

describes the effect a perpendicular magnetic field B. Thus for $B \ll B_c$ or $B \gg B_c$ the magnitude of the UCFs is independent of the Ehrenfest time τ_E^o. However, the form of the crossover between the two limiting cases depends on the Ehrenfest time; the crossover is Lorentzian in the classical limit ($\tau_E^o \gg \tau_D$) and Lorentzian-squared in the RMT limit ($\tau_E^o \ll \tau_D$). The effect of dephasing on UCFs is more complicated [29] and will not be considered here.

C. Adding spatial symmetries to the semiclassical method

We start our discussion of spatial symmetries by explaining the sketches in Figs. 2-5. The relationship between the depicted paths and real classical paths in a chaotic dot is illustrated in Fig. 1. The abstract sketches in Figs. 2-5 neglect all details of the paths except the following essential ones:

- We show that a path crosses the symmetry axis only when it is necessary to understand the nature of the path. For example the paths in Fig. 2(a) going from lead L to lead R are shown to cross the symmetry axis once, when they may in fact cross the symmetry axis any (odd) number of times. Indeed a typical path will cross the symmetry axis every few bounces, and will bounce very many times before escaping into a lead.

- We show when a path comes extremely close in phase space to its symmetric partners (related to it by spatial symmetry). These *effective encounters* play a similar role to those discussed above for weak localization.

In the figures, the right-hand sketches show all paths folded (via the symmetry) into half the system, which emphasizes when a path comes close to its spatially symmetric partner (i.e., its mirror image in systems with a mirror symmetry). As is the case with time-reversal symmetry, pairs of paths that are exactly symmetric have a negligible contribution to the conductance. However, pairs of *approximately* symmetric paths [such as shown in Fig. 2(a)] sum to give a finite contribution. This is also the case for pairs of paths which have some segments which are approximately the same and other segments which are approximately symmetric to each other [such as shown in Fig. 2(b)].

IV. LEFT-RIGHT MIRROR SYMMETRY

First we analyze the case of a perfectly left-right symmetric dot with symmetric leads, $W_{\rm L} = W_{\rm R}$ and therefore $N_{\rm L} = N_{\rm R} \equiv N$. There are three interference contributions to transmission and reflection that exist only because of the symmetry. Two of these contribute to transmission [Fig. 2(a),(b)], while the third contributes to reflection [Fig. 2(c)].

A. Enhanced forward scattering

The contribution of paths of the type in Fig. 2(a) have an effective encounter which is close to the leads. This is analogous to the coherent-backscattering contribution in Ref. [12] (or the D_2, D_3-contributions to the shot noise in Ref. [17]) and we therefore use the same method to treat such paths here. First we note that the behaviour of path γ' is completely determined by that of path γ; the two paths have the same amplitudes, $A_{\gamma'} = A_\gamma$ and the action difference between them is $S_\gamma - S_{\gamma'} = (p_{0\perp} + m\Lambda r_{0\perp}) r_{0\perp}$, where $(r_{0\perp}, p_{0\perp})$ is the component of $\mathbf{Y} - \mathbf{Y}_0$ which is perpendicular to the direction of path γ at $\mathbf{Y}$. This action difference requires hyperbolic chaos and is discussed in detail in the context of coherent backscattering in Ref. [12]. Using the sum rule in Eq. (4), we see that

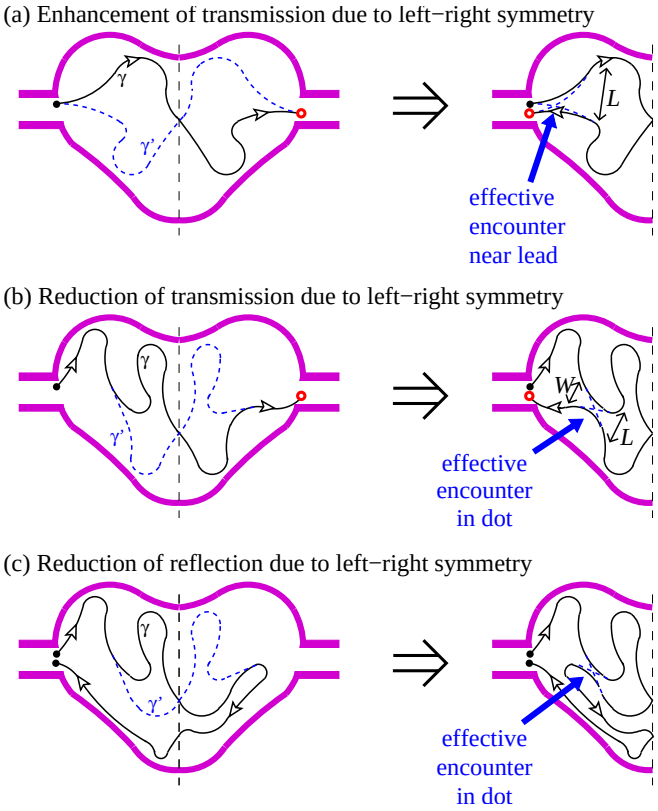

Figure 2: (colour online). Contributions to weak localization due to a left-right mirror symmetry. When we fold the paths into one half of the dot (as shown in the right-hand sketches), paths hitting the symmetry axis are specularly reflected; however, we must keep track of whether the path escapes into the right lead. Thus in those sketches, paths that end on the left lead are marked with solid circles, while those that end on the right lead are marked with open (red) circles. The sketch in (a) is an enhanced forward-scattering contribution, because it enhances transmission through the dot.

the contribution of such paths to the conductance is

$$\langle \delta g \rangle_{\rm LR:a} = (2\pi\hbar)^{-2} \int_{\rm L} {\rm d}\mathbf{Y}_0 \int_{\rm R} {\rm d}\mathbf{Y} \int_0^\infty {\rm d}t \times p_{\rm F} \cos\theta_0 \, \langle \tilde{P}(\mathbf{Y}, \mathbf{Y}_0; t) \rangle \, {\rm Re}\big[{\rm e}^{{\rm i}(S_\gamma - S_{\gamma'})/\hbar} \big]. \quad (10)$$

To perform the average we proceed as for coherent backscattering [12]. Starting at the leads, we define $T'_W(r_{0\perp}, p_{0\perp})$ and $T'_L(r_{0\perp}, p_{0\perp})$ as the time at which the perpendicular distance between γ and γ' reaches W and L, respectively. For times less than $T'_W(r_{0\perp}, p_{0\perp})$, the path segments are paired, and thus their joint survival probability is the same as for a single path (if one path does not touch a lead then the other also does not). For times longer than this the path segments escape independently. We only have contributions if paths γ and γ' diverge from each other in phase space before reconverging at the R lead. For the reconvergence to occur the paths must diverge to a distance of order L (on shorter scales the dynamics are hyperbolic so the reconvergence of diverging paths is not allowed). This means

that the t-integral in Eq. (10) must have a lower cut-off at $2T'_L(r_{0\perp}, p_{0\perp})$.

Now we write the $\mathbf{Y}_0$ integral in Eq. (10) in terms of the relative coordinates $(r_{0\perp}, p_{0\perp})$, using $p_{\rm F}\cos\theta_0 {\rm d}\mathbf{Y}_0 = {\rm d}y_0{\rm d}(p_{\rm F}\sin\theta_0) = {\rm d}r_{0\perp}{\rm d}p_{0\perp}$. Then the $\mathbf{Y}$ integral becomes explicitly independent of $(r_{0\perp}, p_{0\perp})$ and we can write

$$\int_{\rm R}{\rm d}\mathbf{Y}\int_{2T'_L}^{\infty}{\rm d}t\langle\tilde{P}(\mathbf{Y},\mathbf{Y}_0;t)\rangle = \frac{1}{2}\exp[-T'_W/\tau_{\rm D} - 2(T'_L - T'_W)/\tau_{\rm D}], \quad (11)$$

where $T'_{L,W}$ are shorthand for $T'_{L,W}(r_{0\perp}, p_{0\perp})$ and we used the fact that $N_{\rm L} = N_{\rm R}$ to get the prefactor of a half (more generally the prefactor would be $N_{\rm R}/(N_{\rm L}+N_{\rm R})$). For small $(p_{0\perp} + m\Lambda r_{0\perp})$ we get

$$T'_L(r_{0\perp}, p_{0\perp}) \simeq \Lambda^{-1}\ln\left[\frac{m\Lambda L}{|p_{0\perp} + m\Lambda r_{0\perp}|}\right], \quad (12)$$

with $T'_W(r_{0\perp}, p_{0\perp})$ given by the same formula where L is replaced by W. Thus we see that $2(T'_L - T'_W) = \tau_{\rm E}^{\rm c} - \tau_{\rm E}^{\rm o}$, which generates a factor $\exp[-(\tau_{\rm E}^{\rm c} - \tau_{\rm E}^{\rm o})/\tau_{\rm D}]$ and is independent of $(r_{0\perp}, p_{0\perp})$. Substituting these results into Eq. (10) for $\langle\delta g\rangle_{\rm LR:a}$, and recalling that $p_{\rm F}\cos\theta_0{\rm d}\mathbf{Y}_0 = {\rm d}y_0{\rm d}(p_{\rm F}\sin\theta_0) = {\rm d}r_{0\perp}{\rm d}p_{0\perp}$, we get

$$\langle\delta g\rangle_{\rm LR:a} = \frac{{\rm e}^{-(\tau_{\rm E}^{\rm c}-\tau_{\rm E}^{\rm o})/\tau_{\rm D}}}{2(2\pi\hbar)^2}\int_{\rm L}{\rm d}r_{0\perp}{\rm d}p_{0\perp}\,{\rm e}^{-T'_W/\tau_{\rm D}} \times{\rm Re}\big[\exp[{\rm i}(p_{0\perp}+m\Lambda r_{0\perp})r_{0\perp}/\hbar]\big]. \quad (13)$$

We next make the substitution $\tilde{p}_0 = p_{0\perp} + m\Lambda r_{0\perp}$ and evaluate the $r_{0\perp}-$integral over a range of order W. We take the limits on the resulting $\tilde{p}_0$-integral to $\pm\infty$. One can use Euler γ-functions to show that

$$\int_{-\infty}^{\infty}{\rm d}\tilde{p}_0\frac{2\hbar\sin(\tilde{p}_0W/\hbar)}{\tilde{p}_0}\left|\frac{\tilde{p}_0}{m\Lambda W}\right|^{1/(\Lambda\tau_{\rm D})} = 2\pi\hbar\left(\frac{\hbar}{m\Lambda W^2}\right)^{1/(\Lambda\tau_{\rm D})}, \quad (14)$$

the trick in evaluating this integral is to write it as the sum of two integrals from 0 to ∞. The factor of $[\hbar/(m\Lambda W^2)]^{1/(\Lambda\tau_{\rm D})} \simeq \exp[-\tau_{\rm E}^{\rm o}/\tau_{\rm D}]$, where we have dropped $\mathcal{O}(1)$-terms inside a logarithm. This cancels the $\tau_{\rm E}^{\rm o}$-term in the factor $\exp[-(\tau_{\rm E}^{\rm c} - \tau_{\rm E}^{\rm o})/\tau_{\rm D}]$. Collecting terms and evaluating some trivial integrals leads to

$$\langle\delta g\rangle_{\rm LR:a} = \frac{1}{2}\exp[-\tau_{\rm E}^{\rm c}/\tau_{\rm D}]. \quad (15)$$

B. Uniform reduction of transmission and reflection

We now turn to contributions with effective encounters in the dot, Fig. 2(b),(c). We define an effective encounter as being "in the dot" if the parts of path γ on either side of the encounter separate to a distance of at least W before touching any leads. In this case, the ends of path γ are independent of each other, with no correlations in their position, momentum or the time at which they hit a lead. As in the case of the enhanced forward scattering, the path γ and γ' must in fact separate to a distance of order L before they can reconverge. Thus we have two minimal times; $T_{\rm L}(\epsilon)$ for γ and γ' to separate before reconverging [to the right of the encounter in Fig. 2(b)], and $T_{\rm W}(\epsilon)$ for the two parts of γ to separate enough to escape independently into the leads [to the left of the encounter in Fig. 2(b)].

Assuming the encounter is close (i.e. path γ' crosses itself with very small ϵ) and that the classical dynamics are hyperbolic at such small scales, one estimates

$$T_W(\epsilon) \simeq \Lambda^{-1}\ln[\epsilon^{-2}(W/L)^2], \quad (16)$$

with $T_L(\epsilon) \simeq \Lambda^{-1}\ln[\epsilon^{-2}]$. The action difference is $S_\gamma - S_{\gamma'} = E_{\rm F}\epsilon^2/\Lambda$, just as for weak localization [8, 10]. To evaluate the contributions of such paths, the probability $\tilde{P}(\mathbf{Y},\mathbf{Y}_0;t)$ in the sum rule of Eq. (4) is restricted to paths which cross themselves, so that we can write

$$\tilde{P}(\mathbf{Y},\mathbf{Y}_0;t) = \int_{\rm ps}{\rm d}\mathbf{R}_2{\rm d}\mathbf{R}_1\tilde{P}(\mathbf{Y},\mathbf{R}_2;t-t_2) \times\tilde{P}(\mathbf{R}_2,\mathbf{R}_1;t_2-t_1)\tilde{P}(\mathbf{R}_1,\mathbf{Y}_0;t_1), \quad (17)$$

where ps indicates that the integrals are over the phase space of the dot. Here, we use $\mathbf{R} = (\mathbf{r},\phi)$, $\phi\in[-\pi,\pi]$ for phase-space points inside the dot, while $\mathbf{Y}$ lies on the lead as before. We then restrict the probabilities inside the integral to trajectories which cross their mirror image at phase-space positions $\mathbf{R}_{1,2}$ with the first (second) visit to the crossing occurring at time t_1 (t_2). We can write ${\rm d}\mathbf{R}_2 = v_{\rm F}^2\sin\epsilon{\rm d}t_1{\rm d}t_2{\rm d}\epsilon$ and set $\mathbf{R}_2 = (\mathbf{r}'_1, \phi'_1 \pm \epsilon)$, where $\mathbf{r}'_1$ and ϕ'_1 are the mirror images of position $\mathbf{r}_1$ and angle ϕ_1 (thus $\phi'_1 = \pi - \phi_1$). Then the correction to the dimensionless conductance is $\langle\delta g\rangle_{\rm LR:b} = (\pi\hbar)^{-1}\int_{\rm L}{\rm d}\mathbf{Y}_0\int{\rm d}\epsilon\,{\rm Re}\big[e^{i(S_\gamma - S_{\gamma'})/\hbar}\big]\big\langle F(\mathbf{Y}_0,\epsilon)\big\rangle$, with

$$F(\mathbf{Y}_0,\epsilon) = 2v_{\rm F}^2\sin\epsilon\int_{T_L+T_W}^{\infty}{\rm d}t\int_{T_L+\frac{T_W}{2}}^{t-\frac{T_W}{2}}{\rm d}t_2\int_{\frac{T_W}{2}}^{t_2-T_L}{\rm d}t_1 \times p_{\rm F}\cos\theta_0\int_{\rm R}{\rm d}\mathbf{Y}\int_{\rm ps}{\rm d}\mathbf{R}_1\tilde{P}(\mathbf{Y},\mathbf{R}_2;t-t_2) \times\tilde{P}(\mathbf{R}_2,\mathbf{R}_1;t_2-t_1)\tilde{P}(\mathbf{R}_1,\mathbf{Y}_0;t_1). \quad (18)$$

Comparison with Eq. (34) of Ref. [12] shows that this has the same form as the weak localization correction. Thus we only briefly summarize the remainder of the derivation here. Assuming phase space ergodicity for the system, we have

$$\langle F(\mathbf{Y}_0,\epsilon)\rangle = \frac{2v_{\rm F}^2\tau_{\rm D}^2}{2\pi A}\frac{N_{\rm R}}{N_{\rm L}+N_{\rm R}} \times p_{\rm F}\cos\theta_0\,\sin\epsilon\,\exp\big[-T_L(\epsilon)/\tau_{\rm D}\big], \quad (19)$$

with A being the real space volume occupied by the system (the area of the dot). Then the integral over ϵ in $\langle\delta g\rangle_{\rm LR:b}$ takes the form $\mathrm{Re}\int_0^\infty \mathrm{d}\epsilon\,\epsilon^{1+2/(\Lambda\tau_{\rm D})}\,\exp[\mathrm{i}E_{\rm F}\epsilon^2/(\Lambda\hbar)]$, where we have assumed $\epsilon \ll 1$ [12]. The substitution $z = E_{\rm F}\epsilon^2/(\Lambda\hbar)$ immediately yields a dimensionless integral and an exponential term, $\mathrm{e}^{-\tau_{\rm E}^{\rm cl}/\tau_{\rm D}}$ (neglecting as usual $\mathcal{O}[1]$-terms in the logarithm in $\tau_{\rm E}^{\rm cl}$). From this analysis, we find that this interference correction to the conductance is given by $\langle\delta g\rangle_{\rm LR:b} = -\frac{1}{4}\exp[-\tau_{\rm E}^{\rm c}/\tau_{\rm D}]$.

The backscattering contribution in Fig. 2(c) does not directly enter the conductance. However, we must evaluate it if we wish to explicitly show that the theory conserves particles. If interference causes an enhancement of transmission then there must be an associated reduction of reflection; it is the paths in Fig. 2(c) that give this reduction of reflection, which we denote by $\langle\delta R\rangle_{\rm LR:c}$. Inspecting the figure we see that this contribution is of the same form as Eq. (18), but with the $\mathbf{Y}$-integral now over taken over lead L instead of lead R. Thus we find that $\langle\delta R\rangle_{\rm LR:c} = \langle\delta g\rangle_{\rm LR:b}$ so $\langle\delta g\rangle_{\rm LR:a}+\langle\delta g\rangle_{\rm LR:b}+\langle\delta R\rangle_{\rm LR:c} = 0$, which confirms that the theory conserves particles.

C. Asymmetry and dephasing in the dot

We now turn to the effect of deformations of the dot's shape which break the left-right mirror symmetry. We consider two cases; the first is a small deformation of a large proportion of the dot's boundary, see Fig. 3(a), and the second is a large deformation of a small proportion of the dot's boundary, see Fig. 3(b). Other types of deformation can be understood by applying the methodology we introduce for these two cases. In general, the effect of asymmetries on symmetry-induced interference corrections to the conductance is similar to the effect of magnetic fields and dephasing on weak localization for a completely asymmetric dot [10].

Consider the left side of the dot being deformed such that the boundary is rippled, see the sketch in Fig. 3(a). The ripple does not change in time, and has a small amplitude $\delta L < \lambda_{\rm F}$ and long range $W_{\rm asym} \gg \lambda_{\rm F}$ (the latter condition ensures that there is no problem using the semiclassical theory). The simplest such case is when the whole left side of the dot deformed slightly outwards, which corresponds to $W_{\rm asym} \sim L$. Then a path in the left half of the dot which bounces from this portion of the dot boundary will travel a distance of order δL further than its partner in the right half. We assume that this small difference has no significant effect on the classical trajectories but changes the phase acquired along the path and thereby modifies the interference with its symmetry-related partner. Paths are chaotic and regularly switch between the left and right halves of the dot. Thus it is reasonable to assume the length difference between a path segment of time $t \gg \tau_0$ and its mirror image is the sum of many independent random lengths distributed such that $\langle\delta L\rangle = 0$ and $p_{\rm F}^2\langle\delta L^2\rangle \ll \hbar^2$, where the average is over the whole circumference of the dot. Thus the action difference for a path segment of time t (which therefore bounces t/τ_0 times) and its mirror image is $\big\langle \exp[\mathrm{i}(S_\gamma - S_{\gamma'})/\hbar]\big\rangle = \prod_{n=1}^{t/\tau_0}\langle\exp[\mathrm{i}p_{\rm F}\delta L/\hbar]\rangle_n$. Irrespective of the probability distribution of each δL, we can use central limit theorem to tell us that the probability distribution for $(S_\gamma - S_{\gamma'})$ is a Gaussian (Bell-curve) with variance given by the sum of the variances of the individual δLs; thus for times $t \gg \tau_0$ we have

$$\mathrm{var}[S_\gamma - S_{\gamma'}] \simeq (t/\tau_0)\langle\delta L\rangle/\lambda_{\rm F}^2. \tag{20}$$

Thus $\big\langle \exp[\mathrm{i}(S_\gamma - S_{\gamma'})/\hbar]\big\rangle$, which is given by a Gaussian integral over $S_\gamma - S_{\gamma'}$. Evaluating this integral, we find that

$$\big\langle \exp[\mathrm{i}(S_\gamma - S_{\gamma'})/\hbar]\big\rangle = \exp[-\gamma_{\rm asym}t] \tag{21}$$

with decay rate

$$\gamma_{\rm asym} = \langle\delta L^2\rangle/(2\tau_0\lambda_{\rm F}^2). \tag{22}$$

Now we turn to the question of when such random phase differences occur for the interference contributions to conductance. In the contributions we discuss, paths γ and γ' are nearly identical when they enter the effective encounter, while γ is paired with the image of γ' when they exit the encounter. The acquisition of the random phases discussed above only starts to occur once path γ and γ' are a distance $W_{\rm asym}$ or more apart. When the two paths are closer than $W_{\rm asym}$, they do acquire extra phases due to the deformation; however, the phase *difference* between them is negligible. We assume that $W_{\rm asym} \gg \lambda_{\rm F}$, so we can avoid worrying about diffractive scattering from the deformed boundary (it remains smooth at the scale of the Fermi wavelength).

We first consider the effect of asymmetry on the coherent forward-scattering contribution of Fig. 2(a), discussed in Sect. IV A. In this contribution, almost everywhere the paths γ and γ' are the mirror image of each other; the exception is an interval of duration $(t - 2T'_{W_{\rm asym}})$ where the paths separate to a distance of order $W_{\rm asym}$ [here $T'_{W_{\rm asym}}$ is given in Eq. (12) with $W_{\rm asym}$ in place of L]. Thus the integral over time t in Eq. (11) acquires another factor of the form $\exp\big[-\gamma_{\rm asym}(t - 2T'_{W_{\rm asym}})\big]$. Thus asymmetry has a similar effect as dephasing, which contributes a factor of the form $\exp[-\gamma_\phi(t - 2T'_\xi)]$ [30, 31]; here T'_ξ is given by Eq. (12), with the noise correlation length ξ in place of L (see Section III A and references therein). The integral in Eq. (11) is therefore replaced by

$$\begin{aligned}\int_{\rm R}\mathrm{d}\mathbf{Y}\int_{2T'_L}^\infty \mathrm{d}t\langle\tilde{P}(\mathbf{Y},\mathbf{Y}_0;t)\rangle&\\ \times\exp[-(\gamma_{\rm asym}+\gamma_\phi)t]\exp[\gamma_{\rm asym}T'_L+\gamma_\phi T'_\xi]&\\ = \frac{1}{2}\exp[-T'_W/\tau_{\rm D} - 2(T'_L - T'_W)/\tau_{\rm D}]&\\ \times\frac{\exp[-\gamma_\phi\tilde{\tau}-\gamma_{\rm asym}\tilde{\tau}_{\rm asym}]}{1+(\gamma_{\rm asym}+\gamma_\phi)\tau_{\rm D}},&\end{aligned} \tag{23}$$

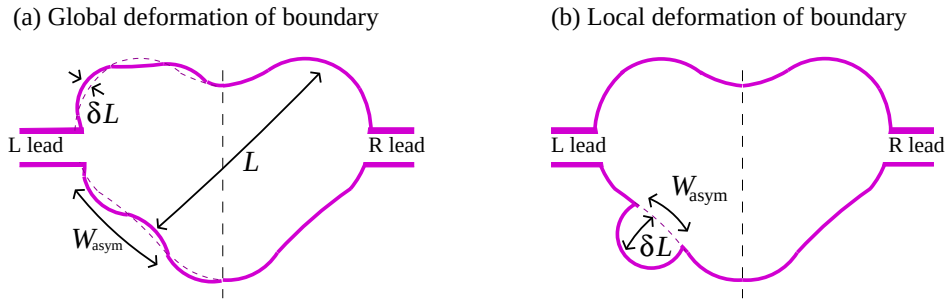

Figure 3: (colour online). Two ways in which the left half of a quantum dot can be deformed away from symmetry with the right half. In (a) the left half is deformed over a long range $W_{\rm asym} \gg \lambda_{\rm F}$ by a gentle ripple of small magnitude $\delta L < \lambda_{\rm F}$. A special case of this is where the whole left-half of the dot is deformed outwards by a distance of order δL, then $W_{\rm asym} \sim L$. In (b) a small part of the boundary of the left half (of width $W_{\rm asym}$) is deformed by a distance $\delta L \gg \lambda_{\rm F}$. In the former case the parameter which controls the deviation from symmetry is $\delta L/\lambda_{\rm F}$ while in the latter case it is $W_{\rm asym}/L$.

where for compactness we define two effective phase correlation times $\tilde{\tau} = 2(T'_L - T'_\xi)$ and $\tilde{\tau}_{\rm asym} = 2(T'_L - T'_{W_{\rm asym}})$ for dephasing and asymmetries, respectively, which take the explicit form

$$\begin{aligned} \tilde{\tau} &= \Lambda^{-1} \ln\left[(L/\xi)^2\right], \\ \tilde{\tau}_{\rm asym} &= \Lambda^{-1} \ln\left[(L/W_{\rm asym})^2\right]. \end{aligned} \tag{24}$$

If the length scale of the deformation of the boundary, $W_{\rm asym}$, is of order L then we can treat $\tilde{\tau}_{\rm asym} \simeq 0$. Similarly, for dephasing, we can treat $\tilde{\tau} \simeq 0$ for $\xi \sim 0$; however, for electron-electron interactions in the dot, $\tilde{\tau}$ is given by the Ehrenfest time $\tau_{\rm E}^{\rm c}$ (see Ref. [29] and Sect. IIIA of Ref. [31], which reviews that work using a similar notation as the present article).

Compared to Eq. (11), Eq. (23) contains an additional constant factor. The remaining derivation of the contribution of coherent forward scattering can therefore proceed exactly as in Section IV A. The final result is $\langle \delta g \rangle_{\rm LR:a} = \frac{1}{2} \exp[-\tau_{\rm E}^{\rm c}/\tau_{\rm D}] \times Z_{\rm LR}(\gamma_{\rm asym}, \gamma_\phi)$, with

$$Z_{\rm LR}(\gamma_{\rm asym}, \gamma_\phi) = \frac{\exp[-\gamma_\phi \tilde{\tau} - \gamma_{\rm asym} \tilde{\tau}_{\rm asym}]}{1 + (\gamma_{\rm asym} + \gamma_\phi)\tau_{\rm D}}. \tag{25}$$

Turning to the other interference contributions for a left-right symmetric dot, Fig. 2(b),(c), we carry out a similar analysis for the parts of the paths which are approximate mirror images of each other. Measuring from the encounter, the paths diverge to a distance $W_{\rm asym}$ apart in a time $T_{W_{\rm asym}}/2$, at which point the asymmetry-induced suppression sets in. Similarly, the paths diverge to a distance ξ apart in a time $T_\xi/2$, at which point the dephasing-induced suppression sets; here the time T_ξ and $T_{\rm W_{asym}}$ are given by Eq. (16) with ξ and $W_{\rm asym}$, respectively, in place of W. The asymmetry suppresses the interference term by a factor $\exp[-\gamma_{\rm asym}(t_2 - t_1 - T_{W_{\rm asym}})]$, while dephasing results in a suppression of the form $\exp[-\gamma_\phi(t_2 - t_1 - T_\xi)]$. Repeating the analysis in Section IV B with these extra terms, we find that $\langle \delta g \rangle_{\rm LR:b}$ and $\langle \delta R \rangle_{\rm LR:c}$ are also suppressed by factors of $Z_{\rm LR}(\gamma_{\rm asym}, \gamma_\phi)$.

It is noteworthy that the expression for $\langle \delta g \rangle_{\rm LR:a}$, $\langle \delta g \rangle_{\rm LR:b}$, and $\langle \delta R \rangle_{\rm LR:c}$ all are independent of the magnetic field, which is quite unlike the weak localization correction given by Eqs. (6,7). The reason for the magnetic-field independence lies in the orientation of trajectory segments in symmetry-related pairs of paths γ, γ'. In all contributions, when both paths are not approximately the same, they are approximately related by taking the mirror image and time-reverse. While the flux enclosed by a path changes its sign by mirror reflection or time reversal, the combined action of both operations results in a path which encloses the same flux as the original path. As a result, the phase induced by the magnetic field is exactly the same for path γ and γ' and drops out of the interference contributions, since the latter only contain the phase difference. This is in stark contrast to the weak localization correction, where the symmetric partner of a path is just its time-reverse, which means the flux enclosed by γ and γ' is opposite (in section V we encounter a similar situation in a dot with inversion symmetry).

We now turn to local deformations as sketched in Fig. 3(b). If neither path γ nor γ' go into the deformed region while they are approximate mirror images of each other, then there is no phase shift, and the contribution is the same as for a perfectly symmetric system. However, if one of the paths enters the deformed region while paired with the mirror image of the other it will immediately acquire a phase difference of $(S_\gamma - S_{\gamma'})/\hbar \gg 1$, and will fluctuate strongly under energy or ensemble averaging. The resulting average $\left\langle \exp[{\rm i}(S_\gamma - S_{\gamma'})/\hbar] \right\rangle$ is still given by Eq. (21), but the decay rate now takes the form

$$\gamma_{\rm asym} = W_{\rm asym}/(2\tau_0 C) = \tau_{\rm D}^{-1} \, (W_{\rm asym}/W), \tag{26}$$

where C is the circumference of the cavity and $W_{\rm asym}$ is the width of the deformation [see Fig. 3(b)]. This asymmetry-induced suppression can only set in once the two paths are a distance of order $W_{\rm asym}$ apart (only then can one path hit the deformation while the other does not), which results in an additional factor $\exp[-(T_L - T_{W_{\rm asym}})/\tau_{\rm D}]$, where $T_{W_{\rm asym}}$ is given by Eq. (16) with $W_{\rm asym}$ in place of W. Following through the calcula-

tion we arrive once again at Eq. (25) but now with $\gamma_{\rm asym}$ given by Eq. (26); $\tilde{\tau}$ and $\tilde{\tau}_{\rm asym}$ are unchanged and given by Eq. (24).

Intriguingly, unlike the dephasing rate Eq. (22) induced by the global asymmetry in Fig. 3(a), the dephasing rate Eq. (26) induced by the localized asymmetry in Fig. 3(b) is wavelength-independent. Thus $W_{\rm asym}$ can be a classical scale (much bigger than $\lambda_{\rm F}$ while remaining less than W) without destroying the symmetry-induced effects. For example, even if $W_{\rm asym} \sim W$ we have $\gamma_{\rm asym}\tau_{\rm D} \sim 1$ and the symmetry-induced effect is only suppressed by a factor of two (then the exponential suppression, $\exp[-\gamma_{\rm asym}\tilde{\tau}_{\rm asym}]$, is almost irrelevant since the exponent contains a logarithm with a small prefactor $(\Lambda\tau_{\rm D})^{-1} \ll 1$).

D. The conductance of a left-right symmetric dot including interference corrections

The total interference correction to the conductance induced by the left-right mirror symmetry is given by $\langle\delta g\rangle_{\rm LR} = \langle\delta g\rangle_{\rm LR:a} + \langle\delta g\rangle_{\rm LR:b} = \frac{1}{4}\exp[-\tau_{\rm E}^{\rm c}/\tau_{\rm D}] \times Z_{\rm LR}(\gamma_{\rm asym},\gamma_\phi)$, with $Z_{\rm LR}(\gamma_{\rm asym},\gamma_\phi)$ given by Eq. (25). Thus a quantum dot with symmetric leads has a total average conductance of

$$\begin{aligned}\langle g\rangle_{\rm LR} &= \langle g\rangle_{\rm D} + \langle\delta g\rangle_{\rm wl} + \langle\delta g\rangle_{\rm LR} \\ &= \frac{N}{2} + \frac{1}{4}\exp[-\tau_{\rm E}^{\rm c}/\tau_{\rm D}]\big[Z_{\rm LR}(\gamma_{\rm asym},\gamma_\phi) - Z(B,\gamma_\phi)\big] \\ &\quad + \mathcal{O}[N^{-1}]. \end{aligned} \tag{27}$$

In the absence of spatial symmetries, the higher-order weak localization corrections (order N^{-1}, etc) were evaluated in Ref. [11]. Symmetry also induces corrections to these orders, but they are beyond the analysis that we carry out here.

As noted in Refs. [22, 23], for perfect left-right mirror symmetry and perfect time-reversal symmetry (no magnetic field) the two interference corrections to the conductance exactly cancel, so that the conductance is given by the classical Drude conductance (5). Interestingly, our calculation shows that this statement remains true for arbitrary dephasing rate and Ehrenfest time, which enter all symmetry-induced corrections with the same functional dependence. However, a magnetic field suppresses the negative weak localization correction, but does not affect the corrections from mirror symmetry. Thus the magneto-conductance curve of a symmetric dot looks like the shifted curve of an asymmetric dot; the shift is positive and equals 1/4 in the RMT limit ($\tau_\phi \gg \tau_{\rm D} \gg \tau_E$). For $W_{\rm asym} \sim L$ (relevant for deformations in Fig. 3(a)) the correction has a Lorentzian dependence on the magnitude of the deformation δL. For $W_{\rm asym} \ll L$, the form of the suppression is more complicated and given in Eq. (25).

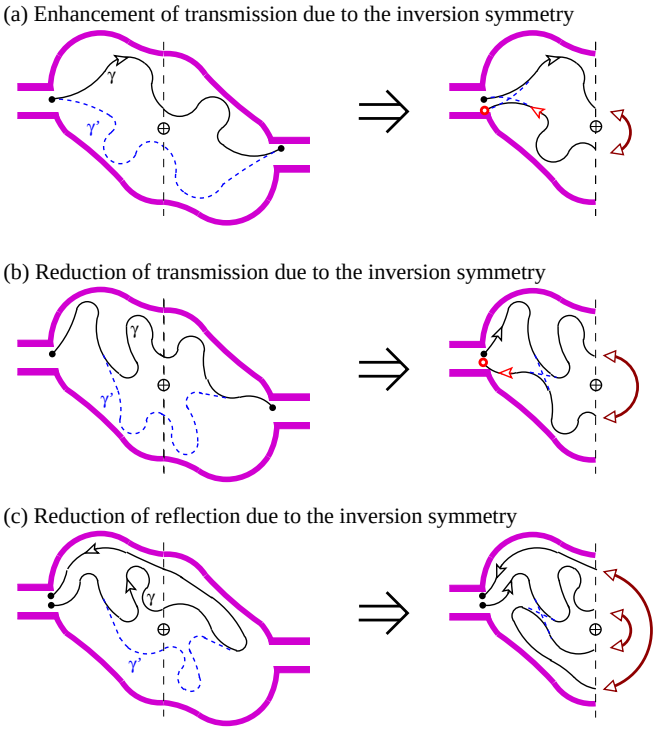

Figure 4: (colour online). Contributions to weak localization due to an inversion symmetry, which is equivalent to symmetry under a 180° rotation about the point indicated by ⊕. In the folded sketches on the right-hand side, paths that end on the left lead are marked with solid circles, while those that end on the right lead are marked with open (red) circles (as in Fig. 2). When we fold all paths into one half of the dot (see the right-hand sketches) by rotating the other half of the dot by 180°, any path which crosses the line between the two halves (dashed line) at (r,p) reappears at $(-r,-p)$, where $r = 0$ is defined as the centre of the inversion symmetry (marked ⊕). The sketch in (a) is an enhanced forward-scattering contribution similar to that in Fig. 2(a).

V. INVERSION SYMMETRY

The effect of inversion symmetry is similar to left-right mirror symmetry. In particular both symmetries map the L lead onto the R lead and vice versa. As the only major difference, inversion symmetry preserves the orientation of closed loops, which results in a different magnetic-field dependence of the interference contributions.

Fig. 4 shows the pairs of paths which give interference corrections due to the inversion symmetry. Here path γ' is the symmetric partner of path γ if the mapping from γ' to γ is inversion plus time-reversal. Comparison with Fig. 2 reveals the similarity of these pairs with the equivalent pairs in a left-right mirror symmetric dot. The only difference is the orientation of loops. Looking at Fig. 4(a) one sees that the flux enclosed by a path is unchanged under inversion, but then changes sign under time-reversal. Thus a path encloses the opposite amount of flux from its "symmetric partner". This is the same

as in a weak localization loop [10] (where the symmetric partner of a path is simply its time-reverse), and so we can expect that the interference corrections induced by the inversion symmetry follow the same Lorentzian magnetic-field suppression [see Eq. (7)].

When performing the calculation of the contributions $\langle \delta g \rangle_{\rm inv}$, the only difference from that for $\langle \delta g \rangle_{\rm LR}$ in Section IV is therefore an extra suppression of the form $\exp[-(t/\tau_0)(B/B_0)^2]$, which is incurred during the time when paths are approximate symmetric partners (rather than being approximately identical). This exponential suppression can be obtained [10] by noting that a path segment acquires a phase $eB\mathcal{A}/h$ between two bounces from the dot's boundary, where $\mathcal{A}$ is the directed area enclosed by the triangle defined by the straight path segment and a third point (say, the point at the centre of the dot). For a chaotic path, $\mathcal{A}$ can be treated as a random variable with $\langle \mathcal{A} \rangle = 0$ and $\langle \mathcal{A}^2 \rangle \sim A^2$, where A is the area of the dot. Assuming the phase acquired between two bounces is small, we can use the central limit theorem to obtain the average value of the phase factor $\exp[{\rm i}\Phi_B(t)]$ for a path segment of duration t (which therefore bounces t/τ_0 times),

$$\begin{aligned} \Big\langle \exp[{\rm i}\Phi_B(t)] \Big\rangle &= \prod_{i=0}^{t/\tau_0} \Big\langle \exp[{\rm i}eB\mathcal{A}/h] \Big\rangle \\ &= \exp[-(t/\tau_0)(B/B_0)^2]. \end{aligned} \tag{28}$$

In all contributions, this factor simply adds to the asymmetry- and dephasing-induced suppression. The final result is

$$\begin{aligned} \langle g \rangle_{\rm inv} &= \frac{N}{2} + \frac{1}{4} {\rm e}^{-\tau_{\rm E}^{\rm c}/\tau_{\rm D}} \left[Z_{\rm inv}(B, \gamma_{\rm asym}, \gamma_\phi) - Z(B, \gamma_\phi) \right] \\ &\quad + \mathcal{O}[N^{-1}] \end{aligned} \tag{29}$$

where we define $N = N_{\rm L} = N_{\rm R}$. The suppression due to a magnetic field, asymmetry or dephasing is given by

$$Z_{\rm inv}(B, \gamma_{\rm asym}, \gamma_\phi) = \frac{\exp[-\gamma_\phi \tilde{\tau} - \gamma_{\rm asym} \tilde{\tau}_{\rm asym}]}{1 + (B/B_{\rm c})^2 + (\gamma_{\rm asym} + \gamma_\phi)\tau_{\rm D}} \tag{30}$$

This is similar to Eq. (25) for a left-right symmetry, but has an extra magnetic-field dependent term in the denominator. Just as for left-right symmetry we have also calculated the contributions to reflection, and verified that particle number is conserved.

VI. UP-DOWN MIRROR SYMMETRY

The case of up-down mirror symmetry is different from the symmetries we have already considered because this symmetry maps each lead onto itself. Figure 5 shows the pairs of paths which contribute to the associated interference corrections; in contrast to the earlier cases there is now only one contribution to transmission [that shown in Fig. 5(c)].

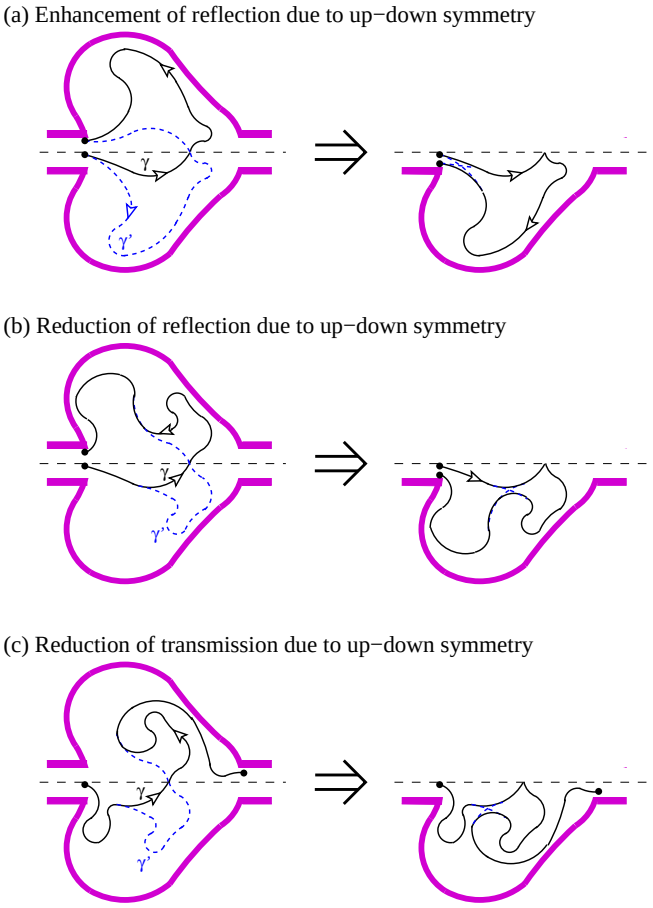

Figure 5: (colour online). Contributions to weak localization due to an up-down mirror symmetry for a dot with symmetric leads. The sketch in (a) is an enhanced backscattering contribution; there are no enhanced forward-scattering contributions (unlike for left-right and inversion-symmetric dots).

Despite the difference in topology from the equivalent pairs in a left-right symmetric dot (shown in Fig. 2), the calculations of the contributions are still similar in the two cases. The integrals we have to evaluate for each contribution in Fig. 5 have the same form as the equivalent contribution in Fig. 2, except that some integrals over lead R now become integrals over lead L, and vice-versa. For symmetric leads (i.e., leads that may have different widths, but must both be centred on the symmetry axis) we then find

$$\begin{aligned} \langle \delta g \rangle_{\rm UD} &= -\frac{N_{\rm L} N_{\rm R}}{(N_{\rm L} + N_{\rm R})^2} \exp[-\tau_{\rm E}^{\rm c}/\tau_{\rm D}^{\rm (UD)}] \\ &\quad \times Z_{\rm UD}(\gamma_{\rm asym}, \gamma_\phi), \end{aligned} \tag{31}$$

where $Z_{\rm UD}(\gamma_{\rm asym}, \gamma_\phi)$ has the same form as $Z_{\rm LR}(\gamma_{\rm asym}, \gamma_\phi)$ given in Eq. (25). For the same reason as for left-right symmetry (but unlike the case of inversion symmetry), there is no magnetic-field dependence. If we sum all the contributions in Fig. 5 we get zero, so the above reduction of transmission is exactly compensated by an enhancement of reflection,

and therefore particles are conserved.

In combination with the weak localization correction, the average conductance of an up-down mirror-symmetric dot is

$$\begin{aligned}\langle g\rangle_{\rm UD} &= \frac{N_{\rm L}N_{\rm R}}{N_{\rm L}+N_{\rm R}} \\ &\quad -\frac{N_{\rm L}N_{\rm R}}{(N_{\rm L}+N_{\rm R})^2}\Bigg[\exp[-\tau_{\rm E}^{\rm c}/\tau_{\rm D}^{\rm (UD)}]\ Z_{\rm UD}(\gamma_{\rm asym},\gamma_\phi) \\ &\quad +\exp[-\tau_{\rm E}^{\rm c}/\tau_{\rm D}]\ Z(B,\gamma_\phi)\Bigg]\ +\mathcal{O}[N_{\rm L,R}^{-1}],\end{aligned} \tag{32}$$

where for simplicity we assume that $\tilde{\tau}$ and $\tilde{\tau}_{\rm asym}$ are small enough to be neglected. For perfect symmetry and vanishing magnetic field, the interference correction to the conductance is exactly twice that of weak localization alone; this is the case for any lead widths, Ehrenfest time or dephasing rate.

VII. FOUR-FOLD SYMMETRY

A quantum dot with four-fold symmetry has all three of the spatial symmetries that we discuss in this article. The interference corrections to the conductance of such a four-fold symmetric quantum dot are simply the sum of the corrections due to each of these three symmetries. The presence of the extra symmetries has no effect on the contributions which do not respect those symmetries, so we can directly take the results we already calculated. The only problem is that we have to avoid double-counting any contributions where a path and its symmetric partner respect more than one of the above symmetries. Luckily such path-pairs are vanishingly rare. For example, to construct a pair of paths related by both left-right and inversion symmetry, one require that both paths go through the left-right mirror axis exactly perpendicular to that axis; only a vanishing small proportion of the paths in the dot do this. Thus

$$\langle\delta g\rangle_{\rm 4F} = \langle\delta g\rangle_{\rm LR}+\langle\delta g\rangle_{\rm UD}+\langle\delta g\rangle_{\rm inv} \tag{33}$$

$$\begin{aligned}&= \frac{1}{4}\exp[-\tau_{\rm E}^{\rm c}/\tau_{\rm D}]\left[Z_{\rm LR}(\gamma_{\rm asym}^{\rm LR},\gamma_\phi)\right. \\ &\quad \left.+Z_{\rm inv}(B,\gamma_{\rm asym}^{\rm inv},\gamma_\phi)-Z_{\rm UD}(\gamma_{\rm asym}^{\rm UD},\gamma_\phi)\right].\end{aligned} \tag{34}$$

For an arbitrary deformation of the dot, one can assume that all three symmetries will be affected about equally, $\gamma_{\rm asym}^{\rm LR}\simeq\gamma_{\rm asym}^{\rm inv}\simeq\gamma_{\rm asym}^{\rm UD}$. However, one could also consider a deformation which respects one of the symmetries, so that the corresponding $\gamma_{\rm asym}$ will be zero, but the other two will be finite (and typically of similar magnitude). For perfect symmetry, we have $\langle\delta g\rangle_{\rm LR}=-\langle\delta g\rangle_{\rm UD}$. Hence in that case $\langle\delta g\rangle_{\rm 4F}=\langle\delta g\rangle_{\rm inv}$ for arbitrary magnetic fields, Ehrenfest time and dephasing rate.

VIII. UNIVERSAL CONDUCTANCE FLUCTUATIONS

In the case of perfect spatial symmetry the universal conductance fluctuations (UCFs) are much easier to analyze than the interference corrections to the conductance itself. Each spatial symmetry doubles the size of every contribution, in exactly the way that introducing time-reversal symmetry doubles the conductance fluctuations in a dot without spatial symmetry (this is also the case in disordered systems, for a review see Ref. [36]). This leads immediately to the results given in Table I.

To see from semiclassics why this is the case, we turn to Fig. 6. Contributions to conductance fluctuations involve two paths, γ_1 and γ_2, from y_0 on lead L to y on lead R, which are completely uncorrelated for part (or all) of their time in the dot. These paths are then paired with another two paths, γ_1' and γ_2' (this time from y_0' on lead L to y' on lead R). If there are no spatial symmetries and no time-reversal symmetry, then there is only one possible pairing which survives averaging: the parts of γ_1 and γ_2 which are not paired with each other must be paired with γ_2' and γ_1' respectively. Time-reversal symmetry induces a second possibility, namely to pair γ_2' and γ_1' with the *time-reverse* of the parts of γ_1 and γ_2 which are not paired with each other. Therefore UCFs in time-reversal symmetric systems are double the magnitude of UCFs in systems without time-reversal symmetry.

The same logic applies to systems with spatial symmetries. If the system has a left-right symmetry, then one can pair γ_2' and γ_1' with the *mirror image* of the parts of γ_1 and γ_2 which are not paired with each other [see Fig. 6(a) for an example of this]. Thus the presence of a left-right symmetry doubles the magnitude of the UCFs. The same additional pairings also occur for up-down and inversion symmetry. For multiple symmetries the effects are multiplicative; assuming that there are n independent symmetries one finds 2^n ways to pair paths, meaning the UCFs are 2^n times larger than for a system with no symmetries. A four-fold symmetry has two independent symmetries (one possible choice is left-right and up-down mirror symmetry, the inversion symmetry being then just a consequence of these two). Fig. 6(b) shows the four possible pairings in such a case.

A. The effect of magnetic fields and asymmetries on UCFs

Asymmetries have a similar effect on paths paired with their mirror-symmetric partner, as magnetic fields have on paths paired with their time-reverse. Path-pairs where each path is the time-reverse of the other (cooperons) decay with a factor of $\exp[-t/\tau_{\rm D}-\tau_0^{-1}(B/B_0)^2t]$, rather than the factor of $\exp[-t/\tau_{\rm D}]$ for pairs where both paths are the same (diffusons). Upon integrating over the length t of such pairs, one sees that for each pair in which the paths are the time-reverse of each other, one gets an

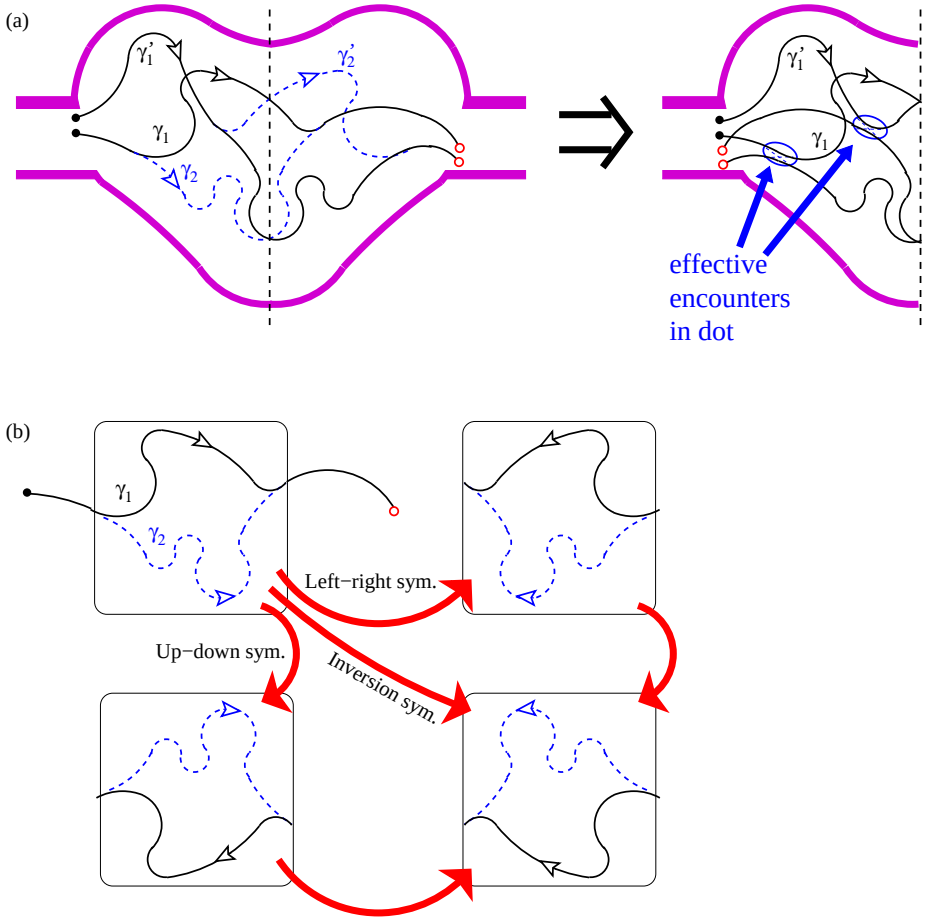

Figure 6: (colour online). (a) A contribution to universal conductance fluctuations in a left-right mirror-symmetric system. On the right we show the same contribution folded into half the dot, such that one can see the two effective encounters (we only show the dashed paths at the encounters). (b) The full list of pairings for path γ_1 and γ_2, with left-right, up-down and inversion symmetry. There are also contributions in which paths are paired with the time-reverse of their images (arrows reversed); indeed (a) is an example of this for a left-right symmetric system.

extra factor of $[1+(B/B_c)^2]^{-1}$ where B_c is given in Eq. (2). Ref. [15] shows that there are two such pairs for zero Ehrenfest time, but only one pair for infinite Ehrenfest time; this observation leads to the result given in Eq. (9).

This methodology can be directly carried over to asymmetries in a spatially symmetric system. Just as for weak localization, pairs where each path is the mirror-symmetric of the other decay with a factor of $\exp[-t/\tau_D - \gamma_{asym}t]$ rather than simply $\exp[-t/\tau_D]$. The asymmetry-induced decay rate γ_{asym} is given by Eq. (22) for asymmetries of the type shown in Fig. 3(a), and by Eq. (26) for asymmetries of the type shown in Fig. 3(b).

We next consider the effect of perpendicular magnetic fields. Looking at the left-right mirror-symmetric paths in Fig. 6(b), we see that they enclose the opposite directed area, so if we pair segments of path γ_2' and γ_1' with the mirror image of segments of γ_1 and γ_2, respectively, then the Aharonov-Bohm flux will be twice that enclosed by paths γ_1 and γ_2. In contrast, if we pair segments of path γ_2' and γ_1' with the *time-reverse* of the mirror image of segments of γ_1 and γ_2, respectively, then the Aharonov-Bohm flux will cancel. Thus we have a factor of $[1+(B/B_c)^2+\gamma_{asym}\tau_D]^{-1}$ for each pair containing paths that are the mirror image of each other, and a factor of $[1+\gamma_{asym}\tau_D]^{-1}$ for each pair containing paths where one is the time-reverse of the mirror image of the other.

As for the contributions in Ref. [15], the zero-Ehrenfest time contributions have two pairs which are not the same, while the infinite-Ehrenfest time contributions have only one. Thus for left-right mirror symmetry we find

$$\mathrm{var}[g]_{LR} = \frac{1}{16}\left[Z^{ucf}(B) + Z^{ucf}_{sym}(B,\gamma^{LR}_{asym})\right], \qquad (35)$$

where $Z^{UCF}(B)$ is given in Eq. (9) and

$$\begin{aligned} Z^{ucf}_{sym}(B,\gamma_{asym}) &= \frac{e^{-\tau^o_E/\tau_D}}{[1+\gamma_{asym}\tau_D]^2} + \frac{e^{-\tau^o_E/\tau_D}}{[1+\gamma_{asym}\tau_D+(B/B_c)^2]^2} \\ &\quad + \frac{1-e^{-\tau^o_E/\tau_D}}{1+\gamma_{asym}\tau_D} + \frac{1-e^{-\tau^o_E/\tau_D}}{1+\gamma_{asym}\tau_D+(B/B_c)^2}. \end{aligned} \qquad (36)$$

For perfect mirror symmetry (as in the absence of spatial symmetries [15]), the magnitude of the UCFs for $B \ll B_c$ and $B \gg B_c$ is independent of the Ehrenfest time, but the crossover from one to the other is given by a Lorentzian in the classical limit ($\tau_E^o \gg \tau_D$) and by a Lorentzian-squared in the random-matrix limit ($\tau_E^o \ll \tau_D$). Similarly for $B \ll B_c$ or $B \gg B_c$, the crossover from symmetric to asymmetric is given by $[1+\gamma_{asym}\tau_D]^{-1}$ in the classical limit and by $[1+\gamma_{asym}\tau_D]^{-2}$ in the random-matrix limit.

The same logic follows for up-down symmetry. In contrast, for the case of an inversion symmetry there is a small difference. Then, if we pair segments of path γ_2' and γ_1' with the image (under the symmetry) of segments of γ_1 and γ_2, respectively, the Aharonov-Bohm flux cancel. If on the other hand we pair segments of path γ_2' and γ_1' with the *time-reverse* of the image (under the symmetry) of segments of γ_1 and γ_2, respectively, then the Aharonov-Bohm will be twice that enclosed by paths γ_1 and γ_2. This means that the contributions to UCFs which survive at finite magnetic field ($B \gg B_c$) for inversion symmetry are exactly those that do not survive for left-right or up-down mirror symmetry, and vice versa. Even though different individual contributions are suppressed for the different symmetries, the total suppression of UCFs by magnetic fields or asymmetries has the same form in all three cases, given by $Z_{sym}^{ucf}(B,\gamma_{asym})$ in Eq. (36), where γ_{asym} measures the deviations from the relevant symmetry.

From this one immediately gets

$$\mathrm{var}[g]_{inv} = \frac{1}{16}\big[Z^{ucf}(B) + Z_{sym}^{ucf}(B,\gamma_{asym}^{inv})\big] \qquad (37)$$

and

$$\mathrm{var}[g]_{UD} = \frac{N_L^2 N_R^2}{(N_L+N_R)^4}\big[Z^{ucf}(B) + Z_{sym}^{ucf}(B,\gamma_{asym}^{UD})\big]. \qquad (38)$$

For four-fold symmetry, the expression for the UCFs contains four terms; the first is from Eq. (9) while each of the others comes from one of the spatial symmetries that a four-fold system respects. Thus

$$\begin{aligned}\mathrm{var}[g]_{4F} \;=\; & \frac{1}{16}\big[Z^{ucf}(B) + Z_{sym}^{ucf}(B,\gamma_{asym}^{LR}) \\ & + Z_{sym}^{ucf}(B,\gamma_{asym}^{inv}) + Z_{sym}^{ucf}(B,\gamma_{asym}^{UD})\big]. \qquad (39)\end{aligned}$$

As we discussed for weak localization, an arbitrary deformation of the dot is likely to affect all three symmetries about equally, with $\gamma_{asym}^{LR} \simeq \gamma_{asym}^{inv} \simeq \gamma_{asym}^{UD}$. However, one could also have a deformation which respects one of the symmetries; then the corresponding γ_{asym} will be zero, while the other two are finite.

For perfect spatial symmetry with $B \ll B_c$ we have $Z_{sym}^{ucf}(B,\gamma_{asym}) = 2$, and a four-fold system has UCFs of magnitude 1/2 irrespective of the Ehrenfest time. For perfect symmetry with $B \gg B_c$ we have $Z_{sym}^{ucf}(B,\gamma_{asym}) = 1$, and a four-fold system has UCFs of magnitude 1/4 irrespective of the Ehrenfest time.

	$B = 0$	$B \gg B_c$
no spatial sym.	COE(M)	CUE(M)
left-right sym.	$A^\dagger$ COE$^2(M/2)$ A	$A^\dagger$ COE(M) A
inversion sym.	$A^\dagger$ COE$^2(M/2)$ A	$A^\dagger$ CUE$^2(M/2)$ A
up-down sym.	C^T COE$^2(M/2)$ C	COE(M)
four-fold sym.	$C^T[A^\dagger$ COE$^2(M/4)$ $A]^2 C$	$A^\dagger$ COE$^2(M/2)$ A

with $A = 2^{-1/2}\begin{pmatrix} 1 & 1 \\ i & -i \end{pmatrix}$ and $C_{i,j} = \delta_{2i-1,j} + \delta_{2i-M,j}$

Table II: Pure random-matrix ensembles for each spatial symmetry, in absence or presence of a magnetic field. The block composition of two identical matrix ensembles of dimension M is abbreviated as $X^2(M) = X(M) \otimes X(M)$. We only consider the case $M \bmod 4 = 0$; in the general case one encounters block composition of ensembles with dimensions that differ at most by 1.

IX. COMPARISON TO RANDOM-MATRIX THEORY

In this section we compare the semiclassical predictions derived in the previous sections to numerical results obtained from a phenomenological random-matrix model. For simplicity, we assume $\tau_E^o \ll \tau_D$ and no dephasing and consider the crossover of quantum-interference effects induced by a magnetic field in cavities of fixed spatial symmetry, as well as the crossover when the magnetic field is fixed but the shape is changed to break one or more spatial symmetries. We concentrate on the case $N_L = N_R = N$.

Our results are based on an efficient interpolation scheme between 'pure' random-matrix ensembles which represent the limiting scenarios of vanishing or strong magnetic field at fully preserved or broken spatial symmetry. We interpolate between these ensembles by means of a procedure which combines the ideas of two constructions used in earlier related works: the stub model of Refs. [37, 38], and the dynamical scattering model of Refs. [39, 40].

The main common feature of our interpolation procedure and the stub model is the idea to introduce a controllable coupling to a symmetry-breaking or magnetic auxiliary system. Ordinarily, this coupling is introduced on the basis of an internal scattering matrix which partially couples to the leads and partially couples to the auxiliary system.

It is beneficial to adapt this approach in a manner which more clearly separates the modifications in the internal dynamics from the coupling to the leads. This can be achieved by first focussing on an $M \times M$-dimensional unitary evolution operator F which represents the internal dynamics of the system. The operator F is taken from a crossover ensemble which we construct by coupling the symmetric system to a symmetry-breaking system, where the flux between the systems is controlled by a param-

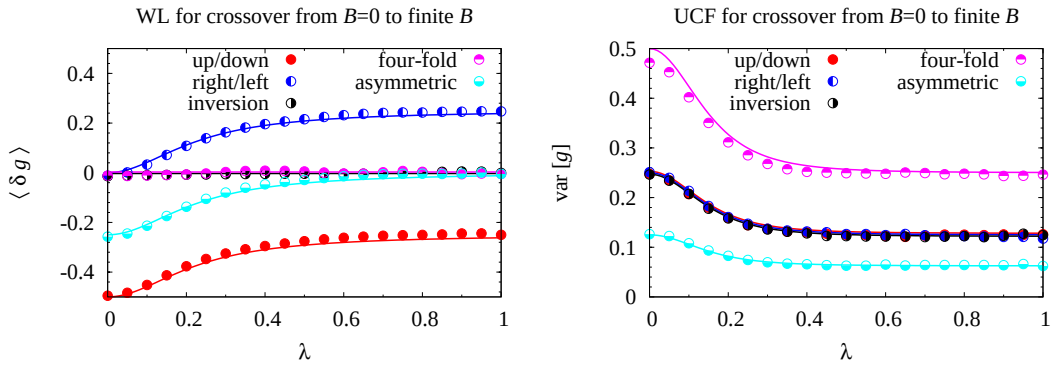

Figure 7: (colour online). Effect of a magnetic field $B = (\lambda/\lambda_c)B_c \simeq \lambda B_0$ on the weak-leak localization correction (left panels) and the conductance fluctuations (right panels) for quantum dots of different spatial symmetry. The solid lines show the universal crossover functions (46) (47), derived in this paper based on semiclassical arguments. The data points show the result of numerical computations based on the interpolation formulae Eqs. (41) and (42) between the random-matrix ensembles tabulated in Tab. II. In these computations, $M = 1000$ and $N = 50$, resulting in $\lambda_c = 1/\sqrt{20}$. Each data point is obtained by averaging over 5000 realizations.

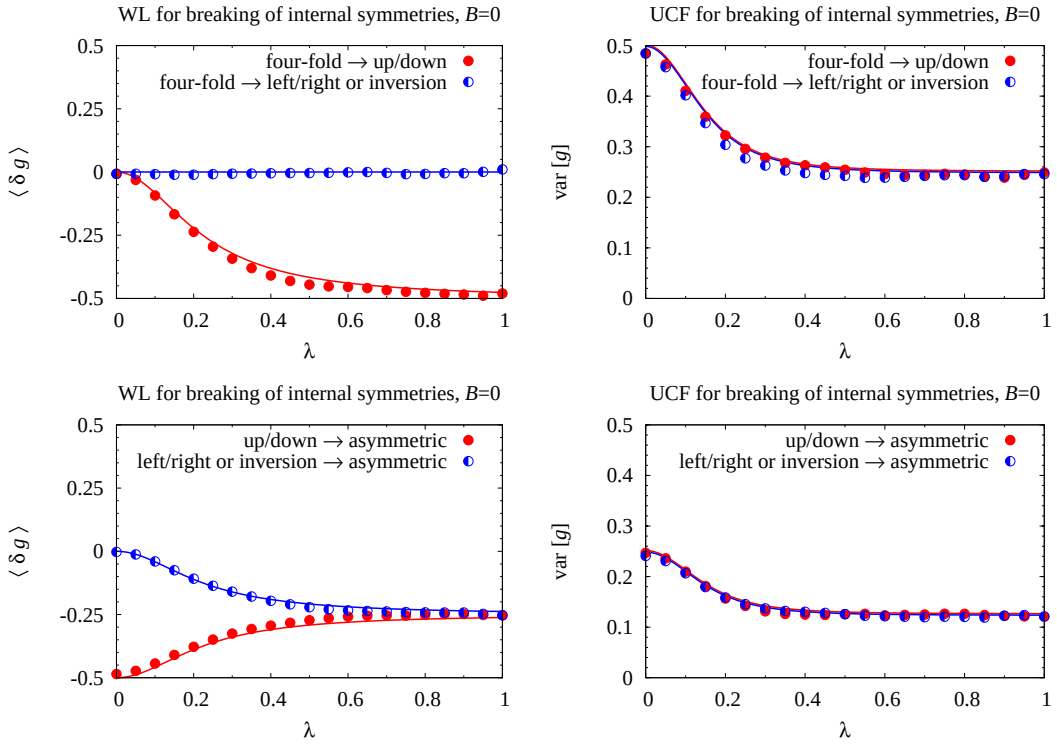

Figure 8: (colour online). Same as Fig. 7, but for transitions induced by the breaking of internal spatial symmetries ($B = 0$).

eter (denoted by λ). The result of this construction is the following simple interpolation formula of the internal operator (given in two equivalent forms):

$$F(\lambda) = (F_0 + \lambda F_1)(1 + \lambda F_1^{-1} F_0)^{-1} \quad (40)$$
$$= (F_0 + \lambda F_1)(F_1 + \lambda F_0)^{-1} F_1. \quad (41)$$

This is a unitary matrix which smoothly interpolates between $F(\lambda = 0) = F_0$ and $F(\lambda = 1) = F_1$.

For reference, Table II lists the pure random-matrix ensembles for the internal operator F in a form in which the leads specified below respect the spatial symmetries (see the second part, Ref. [32], for a generalized model which allows to displace the leads from their symmetric positions). As explained in Appendix A, the form of these matrix ensembles is closely related to the presence or absence of generalized time-reversal symmetry. Drawing pairs F_0, F_1 of matrices at random from two different ensembles listed in Table II delivers a smooth

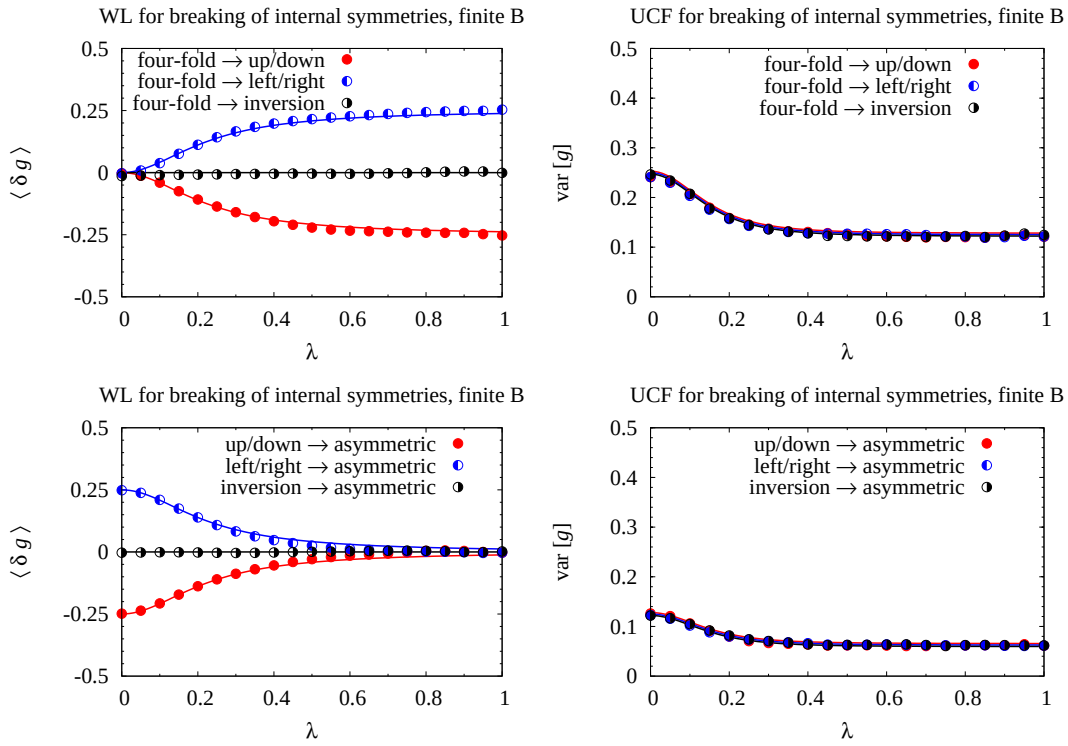

Figure 9: (colour online). Same as Fig. 8, but for a finite magnetic field.

interpolation of the internal dynamics between specified symmetry scenarios.

The phase-coherent transport through the open system can be obtained from the $2N \times 2N$-dimensional scattering matrix $S = \begin{pmatrix} r & t' \\ t & r' \end{pmatrix}$, with blocks containing reflection amplitudes r, r', and transmission amplitudes t, t'. The dimensionless conductance follows from the Landauer formula $g = \mathrm{tr} t^\dagger t$ [21]. Building up on the internal dynamics, we specify the scattering matrix as [39, 40]

$$S = P^T (1 - FQ)^{-1} FP, \tag{42}$$

where

$$P = \begin{pmatrix} 1_{N\times N} & 0_{N\times N} \\ 0_{M/2-N\times N} & 0_{M/2-N\times N} \\ 0_{N\times N} & 1_{N\times N} \\ 0_{M/2-N\times N} & 0_{M/2-N\times N} \end{pmatrix} \tag{43}$$

is a matrix of dimensions $M \times 2N$ which projects onto the leads, while $Q = 1 - PP^T$ projects onto the hard walls where no leakage occurs. Equation (42) lifts the interpolation (41) of the internal dynamics to an interpolation between different scattering matrix ensembles.

While the resulting expressions for the interpolated scattering matrix are quite similar to the stub model, our construction possesses some practical advantages. In particular, the stub model has the deficit that symmetry is not broken for trajectories which avoid the stub (corresponding to a direct transfer from entrance to exit). Total crossover in the stub model therefore can only be achieved in the limit $M \gg N$. That this constraint does not present itself in our procedure is convenient not only because M and N carry precise microscopic meaning, but also because the ratio $M/2N = \tau_D/\tau_0$ represents the dimensionless dwell time featuring in the semiclassical crossover formulae. At the same time, our interpolation procedure avoids the computational overhead which one would encounter by basing the crossover on other microscopic schemes, such as the Pandey-Mehta class of Hamiltonians [21].

In order to determine the physical meaning of the phenomenological parameter λ we consider the universal limit $M \gg N \gg 1$, in which a particle typically undergoes many internal reflections before leaving the system. Each internal reflection probes the broken symmetry, so that we expect that the crossover is essentially completed for small values of λ, on a crossover scale

$$\sqrt{\tau_0/2\tau_D} \simeq \sqrt{N/M} \equiv \lambda_c \tag{44}$$

which scales with the inverse square-root of the dimensionless dwell time. Comparing this crossover acceleration with the effect of a magnetic field in microscopic models (Ref. [21], as well as the semiclassical theory employed in the present paper) allows us to relate the interpolation parameter λ to the magnetic field through the

quantum dot,

$$\lambda = (B/B_c)\lambda_c \simeq B/B_0, \tag{45}$$

where we used Eq. (2). By construction, the crossover scale (44) also applies to interpolation between ensembles of different spatial symmetry.

The semiclassical considerations in this paper predict that the crossover of the weak localization correction and the conductance fluctuations obey a universal functional dependence on λ/λ_c for all types of symmetry breaking, which for $M \gg N$ ($\lambda_c \ll 1$) can be written as

$$\delta g(\lambda) = \delta g(1) + \frac{\delta g(0) - \delta g(1)}{1 + (\lambda/\lambda_c)^2}, \tag{46}$$

$$\mathrm{var}g(\lambda) = \mathrm{var}g(1) + \frac{\mathrm{var}g(0) - \mathrm{var}g(1)}{[1 + (\lambda/\lambda_c)^2]^2}. \tag{47}$$

Here $g(0)$ and $g(1)$ refer to the random-matrix values given in Tab. I.

Figures 7, 8, and 9 compare these analytical predictions to the results of numerical computations for the most important symmetry breaking scenarios. In each figure, the data points are obtained from averaging over 5000 realizations of the corresponding interpolation ensemble. The internal matrix dimension $M = 1000$ and number of channels $N = 50$ translates into a critical value $\lambda_c = 1/\sqrt{20}$ of the interpolation parameter. The solid curves show our analytical predictions, Eqs. (46) and (47). Figure 7 benchmarks the RMT model for the well-studied effects of a magnetic field, demonstrating excellent agreement with a Lorentzian crossover for the weak localization correction and a squared Lorentzian crossover for the universal conductance fluctuations. Figure 8 presents results for breaking of internal symmetries at vanishing magnetic field, while Fig. 9 shows the same transitions for a finite magnetic field. For all symmetry-breaking scenarios the numerical results of the phenomenological random-matrix model are in excellent agreement with the semiclassical predictions.

X. TOWARDS EXPERIMENTAL OBSERVATION

We have investigated the effect of spatial symmetries on transport through chaotic quantum dots, putting significant effort into studying how asymmetries cause a crossover in the weak localization and universal conductance fluctuations (from perfect spatial symmetry to completely broken symmetry). Understanding this crossover is crucial for observing symmetry-induced effects in experiments. Experimenters who believe that their systems are spatially symmetric can demonstrate it by confirming that the interference effects have the deformation dependence that we predict. We are unaware of any experiments in which such symmetry effects have thus far been observed, so here we estimates the conditions under which such observations would be feasible.

The theory presented in this article is for electron transport through quantum dots. Ultra-clean quantum dots are made by placing top gates on two-dimensional electron gases (2DEGs), where typically the electron's wavelength $\lambda_F \sim 50$nm [41]. To observe effects induced by a spatial symmetry, the dot's symmetry must be respected on a scale much less than 50nm. For example, if a typical electron bounces fifty times before escaping, $\tau_D/\tau_0 = 50$, then Eqs. (22,25) indicate that symmetry induced effects will only be significant if imperfections in the dot's boundary are on a scale $\lambda_F/\sqrt{50} \sim 7$nm. This is a substantial experimental challenge, but it is not beyond the realms of possibility.

Note that we have neglected disorder throughout (although it can be included without difficulty as another asymmetry). For quantum dots this is justifiable, due to the remarkable progress in making clean 2DEGs which now have mean-free paths between subsequent impurity scatterings of order of half a millimetre [41]. Consider a dot with 10 modes on each lead, meaning a lead width of $5\lambda_F \simeq 250$nm, with $\tau_D/\tau_0 = 50$. Such a dot has $L \sim 2\mu$m, so the typical distance travelled by an electron between entering and leaving the dot is $v_F\tau_D \sim 100\mu$m. The probability to escape without hitting an impurity is thus about 80%, so we can expect that disorder only reduces the effects discussed here by about 20%. If, in contrast, one takes a dot with 5 modes on each lead and $\tau_D/\tau_0 = 30$ (then $L \sim 0.6\mu$m), one finds a probability to escape without hitting an impurity as high as 96%.

While our theory is for electrons in quantum dots, the results are applicable to any waves in chaotic shaped systems; microwaves in a cavity, ripples on water in a container, vibrations of metal plates, etc. Turning to microwaves in chaotic-shaped cavities [42], we note that the dimensionless conductances that we calculate in this work can be interpreted as a measure of the microwave power transmitted from one lead to the other. Experimentally, the microwave wavelengths are typically a few centimetres, so one only needs to make a cavity within a few millimetres of perfectly symmetric to see a significant effect. This is easily attainable with conventional precision engineering. However we note that our results are for leads carrying many modes, when most experiments to-date on microwave cavities use single-mode leads. In the single-mode case, the interference effects are significantly more complicated than those described here.

XI. CONCLUSIONS

By working with a microscopic theory (rather than the essentially phenomenological RMT) we are not only able to extract the form of the symmetric/asymmetric crossover, we are also able to say how the crossover parameter γ_{asym} depends on the nature of the deformation of the dot. Such knowledge is crucial in determining if

an experimental system is close to being spatially symmetric. We find a remarkable wide variation in this dependence, which for global deformations takes the form of Eq. (22) while for local deformations it is given by Eq. (26). We hope that the semiclassical method developed here will lead to an improved understanding of situations where RMT is hard to apply, such as systems with a mixed phase space for which at present only phenomenological descriptions are available.

In the second of this pair of articles [32], we turn to the problem of a spatially symmetric dot coupled to leads which do not respect the symmetry.

XII. ACKNOWLEDGEMENTS

RW thanks P. Brouwer, P. Marconcini and M. Macucci for interesting and useful discussions. RW and HS are grateful for the hospitality of the Banff International Research Station, where this work was initiated.

Appendix A: GENERALIZED TIME-REVERSAL SYMMETRY

The concept of a generalized time-reversal symmetry is frequently used in the RMT analysis of spatially symmetric systems [43]. We do not explicitly use this concept in our semiclassical calculations but here discuss it briefly because it informs the construction of the RMT ensembles listed in Table II.

A spatially symmetric system which is not symmetric under the standard (momentum-reversing) time-reversal symmetry (such as one with a magnetic field $B \gg B_c$) may still be invariant under the combination of time-reversal and a spatial symmetry. To see this one should note two things; firstly, *all* quantum systems are symmetric under time-reversal if one also changes the sign of the external magnetic field; secondly, mirror symmetries (up-down or left-right symmetry) map a system onto itself with the opposite sign for the external (perpendicular) magnetic field. Thus one immediately sees that an up-down symmetric system will be invariant under the combination of time-reversal and mirror symmetry; this is an example of a generalized time-reversal symmetry. Combining this with the fact that odd (even) transverse lead modes couple only to odd (even) internal states in the dot [22], we obtain the RMT ensembles for up-down symmetry in Table II — odd (even) dot states being those that do (do not) change sign under the up-down mapping. In particular, the generalized time-reversal symmetry manifests itself in the fact that the ensemble is given by combinations of COE matrices for all magnetic fields, even for $B \gg B_c$ where one might naively expect CUE matrices.

The case of a left-right symmetry is a little more involved because acting with the left-right mirror symmetry not only changes the sign of the (perpendicular) magnetic field but also interchanges the leads. Thus the generalized time-reversal symmetry here is a combination of time-reversal symmetry, the left-right symmetry, and the re-labelling of the leads (L$\leftrightarrow$ R) To obtain the ensembles in Table II, one combines this with the fact that all L lead modes couple equally to even and odd dot states, while all R modes have positive coupling to even dot states and negative coupling to odd states. However, once again the presence of the generalized time-reversal symmetry manifests itself in the fact that the ensemble is given by COE matrices even when $B \gg B_c$ (see Table II).

In the case of an inversion symmetry, there is no generalized time-reversal symmetry, and thus the ensemble switches from COE matrices for $B \ll B_c$ to CUE matrices for $B \gg B_c$ (see Table II). The reason for the absence of a generalized time-reversal symmetry is that the inversion symmetry mapping does *not* change the sign of the magnetic field. Thus for $B \gg B_c$, one cannot construct an invariance out of the time-reversal and inversion symmetries.

Having outlined the concept of generalized time-reversal symmetries, one sees that they are most natural in the abstract space used for RMT. However, once we turn to the semiclassical description of concrete systems in which we write contributions in terms of time evolution in phase space, time-reversal symmetry and spatial symmetries are most naturally treated independently from each other.

[1] H. U. Baranger, D. P. DiVincenzo, R. A. Jalabert, and A. D. Stone, Phys. Rev. B **44**, 10637 (1991).
[2] H. U. Baranger, R. A. Jalabert, and A. D. Stone, Chaos **3**, 665 (1993).
[3] A. I. Larkin and D. E. Khmelnitskii, Sov. Phys. Usp. **25**, 185 (1982); D. E. Khmelnitskii, Physica B **126**, 235 (1984).
[4] S. Chakravarty and A. Schmid, Phys. Rep. **140**, 193 (1986).
[5] I. L. Aleiner and A. I. Larkin, Phys. Rev. B **54**, 14423 (1996).
[6] O. Agam, I. Aleiner, and A. Larkin, Phys. Rev. Lett. **85**, 3153 (2000).
[7] M.V. Berry, Proc. R. Soc. London A **400**, 229 (1985).
[8] M. Sieber and K. Richter, Phys. Scr. T **90**, 128 (2001); M. Sieber, J. Phys. A: Math. Gen. **35**, L613 (2002).
[9] S. Müller, S. Heusler, P. Braun, F. Haake, and A. Altland, Phys. Rev. Lett. **93** 014103 (2004). S. Müller, S. Heusler, P. Braun, F. Haake, and A. Altland, Phys. Rev. E **72**, 046207 (2005). S. Heusler, S. Müller, A. Altland, P. Braun, and F. Haake Phys. Rev. Lett. **98**, 044103 (2007).

[10] K. Richter and M. Sieber, Phys. Rev. Lett. **89**, 206801 (2002).

[11] S. Heusler, S. Müller, P. Braun, and F. Haake, Phys. Rev. Lett. **96**, 066804 (2006)

[12] Ph. Jacquod and R. S. Whitney, Phys. Rev. B **73**, 195115 (2006).

[13] S. Rahav and P. W. Brouwer, Phys. Rev. Lett. **96**, 196804 (2006).

[14] P. W. Brouwer and S. Rahav, Phys. Rev. B **74**, 075322 (2006).

[15] P. W. Brouwer and S. Rahav, Phys. Rev. B **75**, 201303(R) (2007).

[16] P. Braun, S. Heusler, S. Müller, and F. Haake, J. Phys. A: Math. Gen. **39**, 159 (2006)

[17] R. S. Whitney and Ph. Jacquod, Phys. Rev. Lett. **96**, 206804 (2006).

[18] S. Müller, S. Heusler, P. Braun, and F. Haake, New J. Phys. **9**, 12 (2007).

[19] O. Bohigas, M. J. Giannoni, and C. Schmit, Phys. Rev. Lett. **52**, 1 (1984).

[20] T. Guhr, A. Müller-Groeling, and H. A. Weidenmüller, Phys. Rep. **299**, 189 (1998).

[21] C. W. J. Beenakker, Rev. Mod. Phys. **69**, 731 (1997).

[22] H. U. Baranger and P. A. Mello, Phys. Rev. B **54**, R14297 (1996)

[23] V. A. Gopar, M. Martínez, P. A. Mello, and H. U. Baranger, J. Phys. A: Math. Gen. **29**, 881 (1996).

[24] M. Martínez and P. A. Mello, Phys. Rev. E **63**, 016205 (2000).

[25] M. Kopp, H. Schomerus, and S. Rotter, Phys. Rev. B **78**, 075312 (2008).

[26] V. A. Gopar, S. Rotter, and H. Schomerus, Phys. Rev. B **73**, 165308 (2006).

[27] R. S. Whitney, P. Marconcini, and M. Macucci, Phys. Rev. Lett. **102**, 186802 (2009).

[28] H. Schomerus and Ph. Jacquod, J. Phys. A **38**, 10663 (2005).

[29] A. Altland, P. W. Brouwer, and C. Tian Phys. Rev. Lett. **99**, 036804 (2007).

[30] C. Petitjean, Ph. Jacquod, and R. S. Whitney, JETP Lett. **86**, 647 (2007).

[31] R. S. Whitney, Ph. Jacquod, and C. Petitjean, Phys. Rev. B **77**, 045315 (2008).

[32] R. S. Whitney, H. Schomerus, and M. Kopp (part II of this series) preprint arXiv:0906.0892.

[33] M. G. Vavilov and A. I. Larkin, Phys. Rev. B **67**, 115335 (2003).

[34] H. Schomerus and J. Tworzydło, Phys. Rev. Lett. **93**, 154102 (2004).

[35] R. S. Whitney, Phys. Rev. B **75**, 235404 (2007).

[36] E. Akkermans and G. Montambaux, *Mesoscopic physics of electrons and photons* (Cambridge University Press, Cambridge, 2007).

[37] P. W. Brouwer, K. M. Frahm, and C. W. J. Beenakker, Waves Random Media **9**, 91 (1999).

[38] P. W. Brouwer, J. N. H. J. Cremers, and B. I. Halperin, Phys. Rev. B **65**, 081302(R) (2002).

[39] Ph. Jacquod, H. Schomerus, and C. W. J. Beenakker, Phys. Rev. Lett. **90**, 207004 (2003).

[40] J. Tworzydło, A. Tajic, H. Schomerus, and C. W. J. Beenakker, Phys. Rev. B **68**, 115313 (2003).

[41] I. P. Radu, J. B. Miller, C. M. Marcus, M. A. Kastner, L. N. Pfeiffer, and K. W. West, Science **320**, 899 (2008)

[42] H.-D. Gräf, H.L. Harney, H. Lengeler, C.H. Lewenkopf, C. Rangacharyulu, A. Richter, P. Schardt, and H.A. Weidenmüller, Phys. Rev. Lett. **69**, 1296 (1992). B. Dietz, T. Friedrich, H.L. Harney, M. Miski-Oglu, A. Richter, F. Schäfer, J. Verbaarschot, and H.A. Weidenmüller, Phys. Rev. Lett. **103**, 064101 (2009).

[43] F. Haake, *Quantum Signatures of Chaos*, 2nd edition (Springer, Berlin, 2001).